

The G-dwarf problem in the Galactic spheroid

R. Caimmi*

December 13, 2017

Abstract

Using two alternative $[O/H]$ - $[Fe/H]$ dependences, the empirical oxygen abundance distribution (EGD) is deduced from two different samples involving (i) 268 K-giant bulge stars (Sadler et al. 1996), and (ii) 149 globular clusters (Mackey & van den Bergh 2005) for which the iron abundance distribution is known, in addition to previous results (Caimmi 2001) related to (iii) 372 solar neighbourhood halo subdwarfs (Ryan & Norris 1991). Under the assumption that each distribution is typical for the corresponding subsystem, the EGD of the Galactic spheroid is determined weighting by mass. The trend is non monotonic, with the occurrence of one minimum and two maxima within the domain. The data are fitted, to an acceptable extent, by simple models of chemical evolution implying both homogeneous and inhomogeneous mixing, provided star formation is inhibited during halo formation and enhanced during bulge formation, with respect to the disk. The theoretical oxygen abundance distribution (TGD) is first determined for the halo and the bulge separately, and then for the Galactic spheroid weighting by mass. Though a G-dwarf problem seems to exist for both the halo and the bulge, it could be alleviated or removed allowing an increasing star formation efficiency during the formation of a Galactic subsystem, which does not necessarily

* *Astronomy Department, Padua Univ., Vicolo Osservatorio 2, I-35122 Padova, Italy*
email: caimmi@pd.astro.it fax: 39-049-8278212

imply gas infall. The results are independent of the power-law initial mass function (IMF) exponent, provided both the lower stellar mass limit and the mass fraction in long-lived stars and remnants per star generation, are suitably changed. Then the effect of star formation inhibiting or enhancing gas is counter-balanced. Simple models implying homogeneous mixing are unable in fitting the empirical age-metallicity relation (EAMR) recently determined from a homogeneous sample of globular clusters (De Angeli et al. 2005), which shows a non monotonic trend characterized by large dispersion. On the other hand, simple models involving inhomogeneous mixing yield a theoretical age-metallicity relation (TAMR) which reproduces the data to an acceptable extent. With regard to gas outflow from the proto-halo, acceptable models make different predictions according if the Galactic spheroid and disk underwent separate or common chemical evolution. In the former alternative, less than one third of the bulge mass outflowed from the proto-halo. In the latter alternative, the existence of an unseen baryonic halo (or equivalent amount of gas lost by the Galaxy) with mass comparable to bulge mass, is necessarily needed. In this view, the outflowing proto-halo gas which remains bound to the Galaxy, makes both the bulge and the disk. The threshold star mass below which the halo is not visible (or an equivalent amount of gas has been lost) is calculated as $m_0 \approx 0.25 m_\odot$ for IMF exponent $p = 2.9$ and $m_0 \approx 0.10 m_\odot$ for $p = 2.35$. Conversely, $p \approx 2.8$ for lower limit stellar mass, $m_{mf} = 0.25 m_\odot$ and $p \approx 2.6$ for $m_0 \approx 0.10 m_\odot$.

keywords - galaxies: evolution - stars: formation; evolution.

1 Introduction

The existence of a G-dwarf problem i.e. the observation of too few metal deficient G dwarfs (or, more generally, of a selected spectral type) with respect to what expected from the Simple model of chemical evolution (e.g., Searle & Sargent 1972; Pagel & Patchett 1975; Haywood 2001) was first established in the solar neighbourhood (van den Bergh 1962; Schmidt 1963). Though in less extreme form, a G-dwarf problem appears to exist in both the halo (e.g., Hartwick 1976; Prantzos 2003) and in the bulge (e.g., Ferreras, Wyse & Silk 2003). In addition, a G-dwarf problem has been detected in both bulge-dominated and disk-dominated galaxies (Henry & Worthey 1999), which is

consistent with the idea that the G-dwarf problem is universal (Worthey, Dorman & Jones 1996).

The deficit of metal-poor stars (with respect to the prediction of the Simple model) may be interpreted in different ways, such as changes in the initial mass function (Schmidt 1963; Adams & Fatuzzo 1996; Bromm 2004; Bromm & Larson 2004; Larson 2005), inflow of unprocessed (Larson 1974) or processed (Thacker, Scannapieco & Davis 2002) material from outside, or evolution with inhomogeneous mixing (Searle 1972; Malinie et al. 1993; Caimmi 2000, 2001b, hereafter quoted as C00¹ and C01, respectively; Oey 2003; Karlsson 2005). For additional alternatives and further details see e.g., Pagel & Patchett (1975); Pagel (1989).

In addition to the G-dwarf problem, a lack of a well-defined empirical age-metallicity relation (EAMR) seems to be established for both the disk solar neighbourhood (e.g., Meusinger, Reimann & Stecklum 1991; Edvardsson et al. 1993; Rocha-Pinto et al. 2000; Feltzing, Holmberg & Hurley 2001; Nordström et al. 2004; Karatas, Bilitz & Schuster 2005) and globular clusters (Salaris & Weiss 2002; De Angeli et al. 2005). The large scatter observed in the EAMR is probably universal, at least with regard to massive enough ($M \gtrsim 10^{10} m_{\odot}$) galaxies, independent of the morphological type.

Inhomogeneous (i.e. implying inhomogeneous gas mixing) models of chemical evolution succeed in both providing a solution to the G-dwarf problem and reproducing substantial scatter exhibited by the EAMR. The current paper aims to investigate if inhomogeneous simple models of chemical evolution are also consistent with the metallicity distribution in the Galactic spheroid, deduced weighting by mass data belonging to subsystems, more specifically solar neighbourhood halo subdwarfs, K-giant bulge stars, and globular clusters. In this view, the next step is to see what constraints are related to the formation and the evolution of the Galaxy.

With regard to halo subdwarfs, the oxygen abundance has been deduced (C01) from data related to a sample of 372 kinematically selected halo stars (Ryan & Norris 1991) after conversion of $[\text{Fe}/\text{H}]$ into $[\text{O}/\text{H}]$ using two alternative empirical relations, involving the presence or absence of $[\text{O}/\text{Fe}]$ plateau for sufficiently low $[\text{Fe}/\text{H}]$ values.

¹With regard to this reference, two points may carefully be kept in mind, namely (i) values of a few parameters must be corrected as explained in Caimmi (2001b), Sect. 3, second paragraph therein, and (ii) the majority of figures do not correspond to the caption, as explained in the erratum (Caimmi 2001a).

With regard to globular clusters and bulge stars, a similar procedure is applied to: (i) a homogeneous sample of 55 objects for which the EAMR is also known (De Angeli et al. 2005), (ii) an inhomogeneous sample of 149 objects (Mackey & van den Bergh 2005), and (iii) a homogeneous sample of 268 bulge K-giant (Sadler, Rich & Terndrup 1996), as reported in Section 2. In addition, it is derived therein a putative oxygen abundance distribution in all halo objects, under the assumption that both globular clusters and field stars underwent a common chemical evolution. The same is made also for the Galactic spheroid, with the inclusion of bulge stars. A comparison with the predictions of simple models, involving homogeneous and inhomogeneous mixing, is made in Section 3 and 4, respectively. The discussion and the conclusion are the subject of Section 5 and 6, respectively.

2 The data

2.1 Empirical age-metallicity relation in globular clusters

Accurate relative ages for a sample of 55 Galactic globular clusters have recently been determined (De Angeli et al. 2005). The ages were obtained by measuring the difference between the horizontal branch and the turnoff in two internally photometrically homogeneous databases with 16 objects in common. The related EAMR is derived from absolute ages and related errors (De Angeli 2005) for objects belonging to a single database. With regard to objects in common where a value and an error exist for each database, the absolute age is calculated as the centre of the intersection of the two intervals, and the error as the corresponding semiamplitude. For instance, 11.42 ∓ 0.34 and 10.96 ∓ 0.60 yield 11.32 ∓ 0.24^2 . Following De Angeli et al. (2005), metallicities are calibrated over two different scales, namely CG (Carretta & Gratton 1997, as extended by Carretta et al. 2001) and ZW (Zinn & West 1984). In addition to the above homogeneous values, a third alternative consists in using the data (taken from different sources) from Harris (1996) catalogue (2003 update), also listed (with one exception) in a recent paper (Mackey & van den Bergh 2005), where five classification types are defined.

²The absolute age could be calculated as a weighted mean, provided the errors available for each database may be related to empirical variances.

With regard to the current sample of 55 objects, three classification types among the above mentioned five shall be retained, namely: BD for bulge/disk clusters (5 objects); OH for old halo clusters (36 objects); and YH for young halo clusters (13 objects). For further details, see Mackey & van den Bergh (2005). An additional cluster (NGC 6366) has to be considered by itself, as belonging to BD type ($[\text{Fe}/\text{H}] > -0.8$) with respect to CG and ZW metallicity scales, and to OH type ($[\text{Fe}/\text{H}] \leq -0.8$) with respect to the value listed in Harris catalogue (Mackey & van den Bergh 2005).

The EAMR for the sample under discussion is represented in Fig. 1, with regard to the above mentioned metallicity scales. An inspection to Fig. 1 discloses the following.

- (i) Age differences related to different metallicity scales are small.
- (ii) The formation of globular clusters in the Galactic halo was a continuous process which span over ≈ 4 Gyr. Low-metallicity halo clusters were generated over ≈ 2 Gyr. Intermediate-metallicity halo clusters were generated over ≈ 4 Gyr. High-metallicity halo clusters and bulge/disk clusters were generated over ≈ 1 Gyr.
- (iii) No clear distinction between “old halo” and “young halo” clusters seems to be in terms of age difference. Perhaps it should be better referring to “primeval halo” and “accreted halo” clusters. The inclusion of YH clusters has no appreciable effect on the EAMR.

Accordingly, the following picture of Galactic evolution may be inferred. Low-metallicity stars formed within the proto-halo and after about 1 Gyr within the proto-bulge/proto-disk. Bulge formation lasted about 1 Gyr, consistent with the absence of bulge stars younger than 10 Gyr (Zoccali et al. 2003), while halo formation ended about 8 Gyr ago, similar to what has been found for the thick disk (Liu & Chaboyer 2000; Ibukiyaua & Arimoto 2002). Then halo and thick disk formation lasted about 4 Gyr and 3 Gyr, respectively. In addition, one has to keep in mind that different specific angular momentum distributions occur in halo-bulge and thick disk-thin disk stars, which implies that the two subsystems had different dynamical evolutions (Ibata & Gilmore 1995).

2.2 Metallicity distribution in globular clusters and field stars

The empirical distribution of oxygen abundance in globular clusters is deduced from a sample of 149 globular clusters where $[\text{Fe}/\text{H}]$ has been determined from different sources (Mackey & van den Bergh 2005) and from a sample of 55 globular clusters where $[\text{Fe}/\text{H}]$ has been determined from a single source (De Angeli et al. 2005). In dealing with simple models of chemical evolution, involving the assumption of instantaneous recycling, the predicted metal abundance has to be compared with the observed oxygen abundance (e.g., Pagel 1989; C00; C01). Unfortunately, oxygen is more difficult than iron to detect, and an empirical relation is needed, to express the former as a function of the latter.

To this respect, a clear dichotomy appears to be among authors who support a plateau in $[\text{O}/\text{Fe}]$ for stars with $[\text{Fe}/\text{H}] \lesssim -1$ (e.g., Carretta, Gratton & Sneden 2000); and those who do not (e.g., Israelian et al. 2001); to get further insight, see the proceedings edited by Barbuy et al. (2001). For exploiting both the above possibilities into consideration, the following relations (C01) shall be used:

$$\left[\frac{\text{O}}{\text{H}}\right] = \begin{cases} \left[\frac{\text{Fe}}{\text{H}}\right] + 0.6 ; & \left[\frac{\text{Fe}}{\text{H}}\right] \leq -1.2 ; & \left[\frac{\text{O}}{\text{H}}\right] \leq -0.6 ; \\ \frac{1}{2} \left[\frac{\text{Fe}}{\text{H}}\right] ; & \left[\frac{\text{Fe}}{\text{H}}\right] \geq -1.2 ; & \left[\frac{\text{O}}{\text{H}}\right] \geq -0.6 ; \end{cases} \quad (1)$$

$$\left[\frac{\text{O}}{\text{H}}\right] = \frac{2}{3} \left[\frac{\text{Fe}}{\text{H}}\right] ; \quad (2)$$

in presence or in absence of $[\text{Fe}/\text{H}]$ plateau, respectively, where the oxygen solar abundance is taken to be $\text{O}_{\odot} = 0.0056$ (Allende-Prieto, Lambert, & Asplund 2001); for further details, see C01.

A number of $[\text{O}/\text{H}]$ - $[\text{Fe}/\text{H}]$ relations lying between those expressed by Eqs.(1) and (2), have been derived from recent investigations (Jonsell et al. 2005; Fulbright, Rich & McWilliam 2005; Garcia Perez et al. 2005; Melendez et al. 2005). To allow comparison with previous results related to halo subdwarfs (C01), Eqs. (1) and (2) shall be used in the current attempt, and hereafter quoted as “in presence” and “in absence” of $[\text{O}/\text{Fe}]$ plateau, respectively, with regard to sufficiently low metallicities, $[\text{Fe}/\text{H}] \lesssim -1$.

On the other hand, extremely metal deficient ($[\text{Fe}/\text{H}] < -4$) stars are known to be oxygen overabundant (e.g., Christlieb et al. 2002; Iwamoto et

al. 2005), $[\text{O}/\text{Fe}] \approx 2.5$ (Bromm & Loeb 2003; Frabel et al. 2006). Then Eqs. (1) and (2) cannot be used in this case, and the chemical evolution shall be restricted to a later epoch where only pop. II star formation occurred, $[\text{Fe}/\text{H}] > -4$, say.

Let us define the oxygen abundance normalized to the solar value, ϕ , as:

$$\log \phi = \log \frac{\text{O}}{\text{O}_{\odot}} = \left[\frac{\text{O}}{\text{H}} \right] ; \quad (3)$$

and let $\Delta \log \phi = \Delta[\text{O}/\text{H}] = [\text{O}/\text{H}]^+ - [\text{O}/\text{H}]^-$ be a logarithmic, oxygen abundance bin deduced from $\Delta[\text{Fe}/\text{H}]$ by use of Eq. (1) or (2). The related, oxygen abundance bin is:

$$\Delta \phi = \Delta^+ \phi + \Delta^- \phi ; \quad \Delta^{\mp} \phi = |\phi - \phi^{\mp}| ; \quad (4a)$$

$$\phi^{\mp} = \exp_{10} \left[\frac{\text{O}}{\text{H}} \right]^{\mp} ; \quad \phi = \frac{\phi^+ + \phi^-}{2} ; \quad (4b)$$

where in general, \exp_{ξ} defines the power of basis ξ and, in particular, \exp defines the power of basis e, according to the standard notation. As in C01, bins in $[\text{Fe}/\text{H}]$ equal to 0.2 dex shall be used (e.g., Norris & Ryan 1991; Huchra, Brodie & Kent 1991; Perrett et al. 2002).

The empirical, differential metallicity distribution (hereafter referred to as EGD) in a selected class of objects, is defined as (Pagel 1989; C00; C01):

$$\psi(\phi \mp \Delta^{\mp} \phi) = \log \frac{\Delta N}{N \Delta \phi} ; \quad (5)$$

where $\Delta \phi$ is the bin width, ΔN is the number of sample objects with oxygen abundance belonging to a bin centered in ϕ , and N is the total number of sample objects. The differential distribution is used instead of the cumulative distribution, as it is a more sensitive test (Pagel 1989) and allows direct comparison between different samples. The uncertainty on ΔN has been evaluated from Poisson errors (e.g., Ryan & Norris 1991), as $\Delta(\Delta N) = (\Delta N)^{1/2}$, and the related uncertainty in the EGD is (e.g., C01):

$$\Delta^{\mp} \psi = |\psi - \psi^{\mp}| = \left| \log \left[1 \mp \frac{(\Delta N)^{1/2}}{\Delta N} \right] \right| ; \quad (6a)$$

$$\psi^{\mp} = \log \frac{\Delta N \mp (\Delta N)^{1/2}}{N \Delta \phi} ; \quad (6b)$$

where ψ^- diverges to $-\infty$ in the limit $\Delta N \rightarrow 1$. For further details, see C01.

The [Fe/H]-[O/H] relation and corresponding mean fractional oxygen abundance, ϕ , and half bin width, $\Delta^\mp\phi$, in presence of [O/Fe] plateau (PP), according to Eq. (1), and in absence of [O/Fe] plateau (AP), according to Eq. (2), respectively, are shown in Tab. 1 for the metallicity range of interest. The EGD derived from the sample studied by De Angeli et al. (2005), using Eqs. (3), (4), (5), (6), is listed in Tab. 2 in presence of [O/Fe] plateau with regard to CG metallicity calibration, and in absence of [O/Fe] plateau with regard to ZW metallicity calibration.

The related plots are shown in Fig. 2, top left and top right, respectively. The dotted vertical line marks the transition from halo (OH, YH) to bulge/disk (BD) morphological type. Bottom left and bottom right panels represent a reduced sample of 42 objects, where YH clusters have been removed. The inclusion of YH clusters (safely stripped from accreted dwarf galaxies like Sagittarius) appears to have no appreciable effect on the EGD. The distribution is bimodal with the occurrence of two maxima, close to the beginning of the evolution and to the transition from halo to bulge/disk morphological type, respectively.

The EGD derived from the sample studied by Mackey & van den Bergh (2005), using Eqs. (3), (4), (5), (6), is listed in Tab. 3 in presence and in absence of [O/Fe] plateau, with regard to metallicity values taken from different sources.

The related plots are shown in Fig. 3, top left and top right, respectively. Bottom left and bottom right panels represent a reduced sample of 107 objects, where only OH clusters have been retained. The inclusion of YH clusters appears to have no appreciable effect on the EGD which, on the other hand, is bimodal with the occurrence of two maxima, close to the beginning of the evolution and to the transition from halo to bulge/disk morphological type, respectively.

The EGD derived from the sample of 268 K-giant bulge stars in Baade's Window studied by Sadler, Rich & Terndrup (1996)³, using Eqs. (3), (4), (5), (6), is listed in Tab. 4 both in presence and in absence of [O/Fe] plateau.

The related plots are shown in Fig. 4, bottom left and bottom right, respectively. Bottom panels represent the EGD deduced from a sample of 372

³The abundance distribution of the sample stars has recently been revised, but with no substantial change (Fulbright et al. 2005, 2006).

Table 1: The [Fe/H]-[O/H] relation and corresponding mean fractional oxygen abundance, ϕ , and half bin width, $\Delta^\mp\phi$, in presence (PP) and in absence (AP) of [O/Fe] plateau. To save space, F stays for [Fe/H] and O for $3[\text{O}/\text{H}]$.

		PP				AP			
F^-	F^+	O^-	O^+	ϕ	$\Delta^\mp\phi$	O^-	O^+	ϕ	$\Delta^\mp\phi$
1.2	1.4	1.8	2.1	4.496	0.515	2.4	2.8	7.443	1.134
1.0	1.2	1.5	1.8	3.572	0.409	2.0	2.4	5.476	0.834
0.8	1.0	1.2	1.5	2.837	0.325	1.6	2.0	4.028	0.613
0.6	0.8	0.9	1.2	2.254	0.258	1.2	1.6	2.963	0.451
0.4	0.6	0.6	0.9	1.790	0.205	0.8	1.2	2.180	0.332
0.2	0.4	0.3	0.6	1.422	0.163	0.4	0.8	1.604	0.244
0.0	0.2	0.0	0.3	1.129	0.129	0.0	0.4	1.180	0.180
-0.2	0.0	-0.30	0.0	0.897	0.103	-0.4	0.0	0.868	0.132
-0.4	-0.2	-0.6	-0.3	0.713	0.087	-0.8	-0.4	0.638	0.097
-0.6	-0.4	-0.9	-0.6	0.566	0.065	-1.2	-0.8	0.470	0.071
-0.8	-0.6	-1.2	-0.9	0.450	0.052	-1.6	-1.2	0.341	0.053
-1.0	-0.8	-1.5	-1.2	0.357	0.041	-2.0	-1.6	0.254	0.039
-1.2	-1.0	-1.8	-1.5	0.284	0.032	-2.4	-2.0	0.187	0.028
-1.4	-1.2	-2.4	-1.8	0.205	0.046	-2.8	-2.4	0.137	0.021
-1.6	-1.4	-3.0	-2.4	0.129	0.029	-3.2	-2.8	0.101	0.015
-1.8	-1.6	-3.6	-3.0	0.081	0.018	-3.6	-3.2	0.074	0.011
-2.0	-1.8	-4.2	-3.6	0.051	0.012	-4.0	-3.6	0.055	0.008
-2.2	-2.0	-4.8	-4.2	0.032	0.007	-4.4	-4.0	0.040	0.006
-2.4	-2.2	-5.4	-4.8	0.020	0.005	-4.8	-4.4	0.030	0.004
-2.6	-2.4	-6.0	-5.4	0.013	0.003	-5.2	-4.8	0.022	0.003
-2.8	-2.6	-6.6	-6.0	0.008	0.002	-5.6	-5.2	0.016	0.002
-3.0	-2.8	-7.2	-6.6	0.005	0.002	-6.0	-5.6	0.012	0.002
-3.7	-3.0	-9.3	-7.2	0.002	0.002	-7.4	-6.0	0.007	0.003

Table 2: The empirical, differential metallicity distribution (EGD) in globular clusters, deduced from a sample of 55 objects studied by De Angeli et al. (2005), in presence of [O/Fe] plateau (PP) with regard to CG metallicity calibration, and in absence of [O/Fe] plateau (AP) with regard to ZW metallicity calibration.

PP					AP				
ϕ	ψ	$\Delta^-\psi$	$\Delta^+\psi$	ΔN	ϕ	ψ	$\Delta^-\psi$	$\Delta^+\psi$	ΔN
0.713	0.000	0.000	0.000	0	0.638	-1.029	∞	0.301	1
0.566	0.000	0.000	0.000	0	0.470	-0.896	∞	0.301	1
0.450	0.025	0.228	0.149	6	0.341	-0.160	0.301	0.176	4
0.357	-0.051	0.301	0.176	4	0.254	-0.629	∞	0.301	1
0.284	0.526	0.148	0.110	12	0.187	-0.019	0.374	0.198	3
0.205	0.469	0.130	0.100	15	0.137	0.592	0.176	0.125	9
0.129	0.095	0.301	0.176	4	0.101	0.885	0.141	0.106	13
0.081	0.391	0.257	0.160	5	0.074	0.807	0.189	0.131	8
0.051	0.591	0.257	0.160	5	0.055	0.816	0.228	0.149	6
0.032	0.570	0.374	0.198	3	0.040	1.016	0.206	0.139	7
0.020	0.293	∞	0.301	1	0.030	0.605	0.533	0.232	2

Table 3: The empirical, differential metallicity distribution (EGD) in globular clusters, deduced from a sample of 149 objects studied by Mackey & van den Bergh (2005), both in presence (PP) and in absence (AP) of [O/Fe] plateau.

PP		AP		$\Delta^- \psi$	$\Delta^+ \psi$	ΔN
ϕ	ψ	ϕ	ψ			
1.422	-1.686	1.604	-1.862	∞	0.301	1
1.129	-1.785	1.180	-1.428	0.533	0.232	2
0.897	-1.185	0.868	-1.294	0.533	0.232	2
0.713	-0.784	0.638	-1.161	0.301	0.176	4
0.566	-0.140	0.470	-0.183	0.135	0.103	14
0.450	-0.040	0.341	-0.049	0.135	0.103	14
0.357	-0.132	0.254	-0.108	0.176	0.125	9
0.284	-0.083	0.187	-0.026	0.189	0.131	8
0.205	0.090	0.137	0.435	0.121	0.094	17
0.129	0.491	0.101	0.769	0.093	0.076	27
0.081	0.490	0.074	0.702	0.121	0.094	17
0.051	0.782	0.055	0.927	0.107	0.086	21
0.032	0.563	0.040	0.641	0.189	0.131	8
0.020	0.559	0.030	0.570	0.257	0.160	5

Table 4: The empirical, differential metallicity distribution (EGD) in K-giant bulge stars in the Baade’s Window, deduced from a sample of 268 objects studied by Sadler et al. (1996), both in presence (PP) and in absence (AP) of [O/Fe] plateau.

PP		AP		$\Delta^- \psi$	$\Delta^+ \psi$	ΔN
ϕ	ψ	ϕ	ψ			
4.496	-2.130	7.443	-2.473	0.533	0.232	2
3.572	-2.030	5.476	-2.339	0.533	0.232	2
2.837	-1.328	4.028	-1.604	0.189	0.131	8
2.254	-0.927	2.963	-1.170	0.125	0.097	16
1.790	-0.569	2.180	-0.778	0.089	0.074	29
1.422	-0.269	1.604	-0.444	0.069	0.060	46
1.129	-0.275	1.180	-0.417	0.079	0.067	36
0.897	-0.175	0.868	-0.284	0.079	0.067	36
0.713	-0.169	0.638	-0.245	0.089	0.074	29
0.566	-0.100	0.470	-0.142	0.093	0.076	27
0.450	-0.201	0.341	-0.210	0.121	0.094	17
0.357	-0.377	0.254	-0.353	0.176	0.125	9
0.284	-0.930	0.187	-0.873	0.533	0.232	2
0.205	-1.385	0.137	-1.040	∞	0.301	1
0.129	-1.185	0.101	-0.907	∞	0.301	1
0.081	0.000	0.074	0.000	0.000	0.000	0
0.051	-0.785	0.055	-0.640	∞	0.301	1

halo subdwarfs in the solar neighbourhood, studied by Ryan & Norris (1991); for further details, see C01.

3 Inferred metallicity distribution in the Galactic spheroid

The Galactic spheroid may safely be conceived as made of three main subsystems, namely: (i) globular clusters, (ii) field halo stars, and (iii) field bulge stars. Let us assume a bulge mass, $M_B = 10^{10}m_\odot$ (e.g., Wyse & Gilmore 1992; Kent 1992; Prantzos & Silk 1998), a (baryonic) halo mass, $M_H = 10^9m_\odot$ (e.g., Carney, Latham & Laird 1990; Wyse & Gilmore 1992), and a ratio of globular clusters to halo mass, $M_{GC}/M_H = 1/100$ (e.g., Li & Burstein 2003), where the above values of bulge and halo mass may safely be used including or not globular clusters. Accordingly, the mass of the Galactic spheroid and the fractional mass of related subsystems read:

$$M = M_{GC} + M_{FH} + M_{FB} = (0.001 + 0.1 + 1) 10^{10}m_\odot = 1.101 m_\odot ; (7a)$$

$$\frac{M_{GC}}{M} = \frac{1}{1101} = 0.0009 ; (7b)$$

$$\frac{M_{FH}}{M} = \frac{100}{1101} = 0.0908 ; (7c)$$

$$\frac{M_{FB}}{M} = \frac{1000}{1101} = 0.9083 ; (7d)$$

where the indices, GC, FH, FB, mean globular clusters, field halo stars, and field bulge stars, respectively.

Let N be the total number of long-lived (i.e. life time longer than the age of the Galaxy) stars in the Galactic spheroid, and ΔN the number of long-lived stars within a selected metallicity bin. The relative frequency, $\Delta N/N$, reads:

$$\frac{\Delta N}{N} = \frac{N_{GC}}{N} \frac{\Delta N_{GC}}{N_{GC}} + \frac{N_{FH}}{N} \frac{\Delta N_{FH}}{N_{FH}} + \frac{N_{FB}}{N} \frac{\Delta N_{FB}}{N_{FB}} ; (8)$$

where $\Delta N_{XY}/N_{XY}$ is the relative frequency belonging to XY subsystem, XY = GC, FH, FB, with regard to the selected metallicity bin. Samples related to different subsystems may be (and in fact are) made of different objects, provided each sample is statistically significant.

With regard to field (halo and bulge) stars, let us define a selected spectral class of long-lived stars as belonging to a selected mass range, $m_1 \leq m \leq m_2$, and suppose it does not significantly depend on the evolution, as in disk stars (Rocha-Pinto & Maciel 1997). Then the fractional number of stars belonging to an assigned mass range, equals the fractional number of stars belonging to the whole mass domain, provided the initial mass function (IMF) did not significantly change within the Galactic spheroid. Accordingly, the following relation holds:

$$\left(\frac{N_{XY}}{N}\right)_{m_1, m_2} = \frac{N_{XY}}{N} \quad XY = \text{GC, FH, FB} ; \quad (9)$$

and, on the other hand:

$$\frac{N_{XY}}{N} = \frac{\bar{m}_{XY} N_{XY}}{\bar{m} N} = \frac{M_{XY}}{M} ; \quad (10)$$

where \bar{m}_{XY} and \bar{m} are the mean mass of long-lived stars in XY subsystem and in the Galactic spheroid, respectively, and $\bar{m}_{XY} = \bar{m}$ owing to the assumption of universal IMF.

The combination of Eqs. (8), (9), and (10) yields:

$$\frac{\Delta N}{N} = \frac{M_{\text{GC}}}{M} \frac{\Delta N_{\text{GC}}}{N_{\text{GC}}} + \frac{M_{\text{FH}}}{M} \frac{\Delta N_{\text{FH}}}{N_{\text{FH}}} + \frac{M_{\text{FB}}}{M} \frac{\Delta N_{\text{FB}}}{N_{\text{FB}}} ; \quad (11)$$

and the related uncertainty is obtained using the standard formula of linear propagation of errors together with evaluation of Poisson errors (e.g., Ryan & Norris 1991), $\Delta(\Delta N_{XY}) = (\Delta N_{XY})^{1/2}$. The result is:

$$\Delta \frac{\Delta N}{N} = \frac{M_{\text{GC}}}{M} \frac{(\Delta N_{\text{GC}})^{1/2}}{N_{\text{GC}}} + \frac{M_{\text{FH}}}{M} \frac{(\Delta N_{\text{FH}})^{1/2}}{N_{\text{FH}}} + \frac{M_{\text{FB}}}{M} \frac{(\Delta N_{\text{FB}})^{1/2}}{N_{\text{FB}}} ; \quad (12)$$

which may explicitly be calculated using Eqs. (7) and the data listed in Tab. 3, Tabs. 1-2 in C01, and Tab. 4, concerning globular clusters, field halo stars, and field bulge stars, respectively.

The EGD in stars of the Galactic spheroid results from the combination of Eqs. (5), (6), and (11), as:

$$\psi = \log \left[\frac{M_{\text{GC}}}{M} \frac{\Delta N_{\text{GC}}}{N_{\text{GC}} \Delta \phi} + \frac{M_{\text{FH}}}{M} \frac{\Delta N_{\text{FH}}}{N_{\text{FH}} \Delta \phi} + \frac{M_{\text{FB}}}{M} \frac{\Delta N_{\text{FB}}}{N_{\text{FB}} \Delta \phi} \right] ; \quad (13a)$$

$$\Delta^{\mp}\psi = \left| \log \left[1 \mp \frac{\Delta(\Delta N/N)}{\Delta N/N} \right] \right| ; \quad (13b)$$

$$\psi^{\mp} = \log \sum_{XY} \left[\frac{M_{XY}}{M} \frac{\Delta N_{XY} \mp (\Delta N_{XY})^{1/2}}{N_{XY} \Delta \phi} \right] ; \quad (13c)$$

where $XY = \text{GC, FH, FB}$.

As a first application of Eqs. (11), (12), and (13), let us take into consideration the light Galactic spheroid, made of globular clusters and field halo stars. To this aim, the globular cluster sample (Mackey & van den Bergh 2005) has been reduced to $N = 148$ with the exclusion of Liller I owing to its high metal content, $[\text{Fe}/\text{H}] = 0.22$, which exceeds the maximum metallicity in solar neighbourhood halo subdwarf sample (Ryan & Norris 1991) used here. The resulting EGD is listed in Tab.5 both in presence and in absence of $[\text{O}/\text{Fe}]$ plateau. The related plots are shown in Fig. 5 (top panels), left and right, respectively.

A second application concerns the massive Galactic spheroid, including globular clusters, field halo stars, and field bulge stars. The resulting EGD is listed in Tab.6 both in presence and in absence of $[\text{O}/\text{Fe}]$ plateau. The related plots are shown in Fig. 5 (bottom panels), left and right, respectively.

The EGD in the Galactic spheroid is similar to its counterpart related to globular cluster subsystem, Fig. 3, which is bimodal with the occurrence of two distinct maxima, and a minimum soon before the transition from halo to bulge/disk morphological type, represented by a dotted vertical line. It is apparent that (closed or open) simple models of chemical evolution cannot provide a satisfactory explanation to a bimodal EGD, and a different model is needed.

Accordingly, let us suppose the halo and the bulge underwent distinct chemical evolutions, calculate the related theoretical differential metallicity distribution (hereafter referred to as TGD) in a selected spectral class of long-lived stars, the resulting TGD, and compare with its empirical counterpart. To this aim, simple models implying both homogeneous and inhomogeneous mixing shall be used, as in C01.

Table 5: The empirical, differential metallicity distribution (EGD) in the light Galactic spheroid (globular clusters and field halo stars), deduced from a sample of 148 globular clusters (Mackey & van den Bergh 2005) and a sample of 372 field halo subdwarfs (Ryan & Norris 1991), both in presence (PP) and in absence (AP) of [O/Fe] plateau.

PP		AP		$\Delta^- \psi$	$\Delta^+ \psi$	$\frac{\Delta N}{N}$	$\Delta \frac{\Delta N}{N}$
ϕ	ψ	ϕ	ψ				
0.958	-2.048	0.951	-2.167	1.336	0.291	0.003	0.003
0.713	-1.080	0.638	-1.156	0.258	0.161	0.014	0.006
0.566	-0.821	0.470	-0.864	0.202	0.137	0.020	0.007
0.450	-0.496	0.345	-0.505	0.148	0.110	0.033	0.009
0.357	-0.367	0.254	-0.342	0.142	0.107	0.035	0.010
0.284	0.062	0.187	0.120	0.092	0.076	0.075	0.014
0.205	0.096	0.137	0.441	0.072	0.062	0.116	0.018
0.129	0.371	0.101	0.650	0.066	0.057	0.137	0.019
0.081	0.653	0.074	0.865	0.059	0.052	0.166	0.021
0.051	0.707	0.055	0.852	0.071	0.061	0.118	0.018
0.032	0.792	0.040	0.870	0.082	0.069	0.091	0.016
0.020	0.840	0.030	0.852	0.100	0.081	0.064	0.013
0.013	0.980	0.022	0.925	0.107	0.086	0.056	0.012
0.008	0.972	0.016	0.850	0.141	0.106	0.035	0.010
0.005	0.961	0.012	0.773	0.189	0.131	0.021	0.008
0.002	0.700	0.007	0.385	0.228	0.149	0.016	0.007

Table 6: The empirical, differential metallicity distribution (EGD) in the massive Galactic spheroid (globular clusters, field halo stars, and field bulge stars), deduced from a sample of 149 globular clusters (Mackey & van den Bergh 2005), a sample of 372 field halo subdwarfs (Ryan & Norris 1991), and a sample of 268 field K-giant bulge stars (Sadler et al. 1996), both in presence (PP) and in absence (AP) of [O/Fe] plateau.

PP		AP		$\Delta^- \psi$	$\Delta^+ \psi$	$\frac{\Delta N}{N}$	$\Delta \frac{\Delta N}{N}$
ϕ	ψ	ϕ	ψ				
4.496	-2.172	7.443	-2.515	0.533	0.232	0.007	0.005
3.572	-2.072	5.476	-2.381	0.533	0.232	0.007	0.005
2.837	-1.370	4.028	-1.646	0.189	0.131	0.028	0.010
2.254	-0.969	2.963	-1.211	0.125	0.097	0.055	0.014
1.790	-0.611	2.180	-0.820	0.089	0.074	0.100	0.019
1.422	-0.310	1.604	-0.486	0.069	0.060	0.159	0.023
1.129	-0.316	1.180	-0.458	0.080	0.068	0.125	0.021
0.897	-0.217	0.868	-0.326	0.079	0.067	0.125	0.021
0.713	-0.205	0.638	-0.281	0.091	0.075	0.102	0.019
0.566	-0.134	0.470	-0.176	0.095	0.078	0.095	0.019
0.450	-0.221	0.341	-0.230	0.122	0.095	0.062	0.015
0.357	-0.376	0.254	-0.352	0.173	0.127	0.034	0.011
0.284	-0.673	0.187	-0.615	0.259	0.161	0.014	0.006
0.205	-0.819	0.137	-0.474	0.195	0.134	0.014	0.005
0.129	-0.561	0.101	-0.282	0.171	0.122	0.016	0.005
0.081	-0.384	0.074	-0.172	0.059	0.052	0.015	0.002
0.051	-0.211	0.055	-0.066	0.192	0.132	0.014	0.005
0.032	-0.245	0.040	-0.167	0.082	0.069	0.008	0.001
0.020	-0.197	0.030	-0.185	0.100	0.081	0.006	0.001
0.013	-0.057	0.022	-0.112	0.107	0.086	0.005	0.001
0.008	-0.065	0.016	-0.187	0.141	0.106	0.003	0.001
0.005	-0.076	0.012	-0.265	0.189	0.131	0.002	0.001
0.002	-0.337	0.007	-0.653	0.228	0.149	0.001	0.001

4 Homogeneous simple models

With regard to homogeneous simple models with star formation inhibiting gas (e.g., Hartwick 1976; C00; C01), the TGD is represented as a straight line (e.g., Pagel 1989; C00; C01):

$$\psi(\phi) = \log \frac{dN}{N d\phi} = a\phi + b \quad ; \quad (14)$$

and the explicit expression of the coefficients, a and b , reads:

$$a = -\frac{1}{\ln 10} \frac{O_{\odot}}{\hat{p}''} \quad ; \quad (15)$$

$$b = \log \left(\frac{\mu_o}{\mu_o - \mu_f} \frac{O_{\odot}}{\hat{p}''} \right) - a\phi_o \quad ; \quad (16)$$

where O_{\odot} is the solar oxygen abundance, \hat{p}'' the effective (oxygen) yield, μ the (allowing star formation) gas mass fraction, and the indices, o and f , denote the beginning and the end of evolution, respectively.

The oxygen abundance, O , may be related, to a good extent, to the gas mass fraction, μ , as (e.g., C00; C01):

$$O - O_0 = -\hat{p}'' \ln \frac{\mu}{\mu_0} \quad ; \quad (17)$$

$$\hat{p}'' = \frac{\hat{p}}{1 + \kappa} \quad ; \quad (18)$$

where \hat{p} , is the real (oxygen) yield and κ is the ratio of (inhibiting star formation) gas mass fraction to long-lived star and remnant mass fraction. In addition, the following assumptions have been made: (i) instantaneous recycling; (ii) universal power-law IMF; and (iii) gas inhibition from forming stars at a rate proportional to the star formation rate. For further details see e.g., Hartwick (1976); Pagel (1989); C00; C01.

A deeper analysis shows that, given a simple model with star formation inhibiting gas, long-lived lower stellar mass limit, m_{mf} , and inhibition parameter, κ , it is equivalent to a simple model with same values of independent parameters except the above mentioned two, $(m_{mf})_1 \leq m_{mf}$ and $\kappa_1 = 0 \leq \kappa$; and vice versa. Accordingly, the related yield, \hat{p}_1 , has the same value as the

effective yield, \hat{p}' , expressed by Eq. (18). For an exhaustive discussion, see C01.

Simple models with star formation inhibiting gas (Hartwick 1976) can be generalized to negative values of the inhibition parameter, $\kappa < 0$, where star formation is enhanced by additional gas with same composition as the pre-existing one, at a rate:

$$\frac{dD}{dt} = \alpha\kappa \frac{dS}{dt} ; \quad \kappa < 0 ; \quad (19)$$

which corresponds to a total amount:

$$D(t) - D_o = \alpha\kappa[S(t) - S_o] = \kappa[s(t) - s_o] ; \quad \kappa < 0 ; \quad (20)$$

where D , S , and s represent the mass fraction in additional gas, stars formed, and long-lived stars and remnants, respectively, and α is the mass fraction of a star generation which remains locked up in long-lived stars and remnants.

The additional gas may be conceived as inflowing from outside, with same composition as the pre-existing gas, and entirely turned into stars. Accordingly, the mass fraction with respect to the original system, $\mu + s$, reads:

$$\mu(t) + s(t) = 1 - D(t) ; \quad \kappa < 0 ; \quad (21)$$

and the combination of Eqs. (20) and (21) yields:

$$s - s_o = \frac{\mu_0 - \mu}{1 + \kappa} ; \quad (22)$$

$$D - D_o = \frac{\kappa(\mu_o - \mu)}{1 + \kappa} ; \quad (23)$$

finally, the related distribution of metal abundance in long-lived stars can be determined following a standard procedure (e.g., Pagel & Patchett 1975; Caimmi 1981), as done in C01. In fact, all the considerations made in C01 (Appendix C) are independent of the sign of the inhibition parameter, κ , and Theorem 1 therein may be generalized in the following way.

Theorem *Given a simple model of chemical evolution with star formation inhibiting gas, long-lived (i.e. life time longer than the age of the system) lower stellar mass limit, m_{mf} , and inhibition parameter, κ (where positive and negative values correspond to star formation inhibiting and enhancing*

gas, respectively), it is equivalent to any model of the same kind and with same values of parameters, except the above mentioned two, $(m_{mf})_n$ and κ_n , which are defined by the relations:

$$(m_{mf})_1 \leq (m_{mf})_n \leq m_{mf} \ ; \quad \kappa \geq 0 \ ; \quad (24a)$$

$$(m_{mf})_n \leq (m_{mf})_1 \leq m_{mf} \ ; \quad -1 < \kappa \leq 0 \ ; \quad (24b)$$

$$\frac{1 + \kappa_n}{1 + \kappa} = \frac{\hat{p}_n}{\hat{p}} \ ; \quad (25)$$

where $(m_{mf})_1$ is related to $\kappa_n = 0$, i.e. star formation neither inhibiting nor enhancing gas.

Aiming to an application of the above results to the chemical evolution of the Galactic spheroid, the value of the real normalized yield, \hat{p}/O_\odot , the long-lived star and remnant mass fraction in a star generation, α , and the lower stellar mass limit, m_{mf} , shall be taken from a fit to the EGD in the disk solar neighbourhood (C00) with regard to a solar oxygen abundance, $O_\odot = 0.0056$ (C01).

Two extreme values of the power-law IMF exponent, p , shall be considered, namely: (i) $p = 2.9$, which is a fit to the IMF determined by Scalo (1986) or Miller & Scalo (1979), for $m \gtrsim m_\odot$, and provides a good approximation also in terms of oxygen production (Wang & Silk 1993); in fact, a different model (with respect to the current one) for the chemical evolution of the Galactic halo also requires a Miller-Scalo IMF to fit the data (Lu et al. 2001), and (ii) $p = 2.35$, which coincides with the IMF determined by Salpeter (1955). Different fits to the EGD in the Galactic spheroid, with respect to the solar neighbourhood, would imply star formation inhibiting or enhancing gas. For deeper insight into the model, see C00, C01.

Input parameters which remain fixed are listed in Tab.7, where the indices, 2.9 and 2.35, denote the value of the power-law IMF exponent used in computing the corresponding quantities. The initial oxygen abundance assumed for field halo stars, $\phi_{oH} = 0.001$, is consistent with a lower limit deduced from theoretical considerations, to allow pop. II star formation (Bromm & Loeb 2003).

Different models can be obtained by changing a single remaining input parameter, which can be chosen as the normalized effective yield, \hat{p}''/O_\odot , or the slope of the TGD, a , conform to Eqs. (14) and (15).

Table 7: Values of input parameters of simple homogeneous models with star formation inhibiting or enhancing gas. The indices, 2.9 and 2.35, denote the value of the power-law IMF exponent used in computing the corresponding quantities. The indices, H and B, denote halo and bulge field star subsystem, respectively.

$\hat{p}/O_{\odot} \cdot 10$	7.3722
$(\widetilde{m}_{mf})_{2.9} \cdot 10$	3.4235
$(\widetilde{m}_{mf})_{2.35} \cdot 10^3$	6.9136
$\alpha_{2.9} \cdot 10$	7.3666
$\alpha_{2.35} \cdot 10$	8.9104
μ_o	1
s_o	0
D_o	0
$\phi_{oH} \cdot 10^3$	1
ϕ_{oB}	0.20
ϕ_{fH}	1
ϕ_{fB}	5.5
$O_{\odot} \cdot 10^3$	5.6

Table 8: Values of parameters related to homogeneous simple models with star formation inhibiting or enhancing gas, corresponding to linear fits to the empirical differential metallicity distribution (EGD) in halo (H) and bulge (B) field stars, plotted in Fig. 4. The mean oxygen abundance (normalized to the solar value) of stars at the end of evolution is denoted as $\bar{\phi}$. Positive and negative κ values mean star formation inhibiting and enhancing gas, respectively. Positive and negative D values mean star formation inhibiting gas and stars formed from additional gas with same composition as the pre-existing gas, respectively. Mass fractions are normalized to the initial mass.

	H1	H2	B1	B2
\hat{p}''/O_{\odot}	1.3363 E-1	9.2288 E-2	1.0857 E-0	8.1430 E-1
a	-3.2500 E-0	-4.7059 E-0	-4.0000 E-1	-5.3333 E-1
b	8.7771 E-1	1.0396 E-0	1.1048 E-1	2.3465 E-1
κ	4.5169 E-0	6.9883 E-0	-3.2099 E-1	-9.4658 E-2
μ_f	5.6657 E-4	1.9899 E-5	7.5858 E-3	1.4905 E-3
s_f	1.8116 E-1	1.2518 E-1	1.4616 E-0	1.1029 E-0
D_f	8.1828 E-1	8.7480 E-1	-4.6915 E-1	-1.0440 E-1
$\bar{\phi}$	1.3406 E-1	9.3268 E-2	1.2452 E-0	1.0064 E-0

A few cases are listed in Tab. 8, related to halo (H) and bulge (B) field stars, respectively, where $\bar{\phi}$ represents the mean oxygen abundance (normalized to the solar value) of stars at the end of evolution. Positive and negative κ values mean star formation inhibiting and enhancing gas, respectively. Positive and negative D values mean star formation inhibiting gas and stars formed from additional gas with same composition as the pre-existing gas, respectively.

It is apparent that halo and bulge models demand star formation inhibiting and enhancing gas, respectively, to maintain (i) universal power-law IMF, and (ii) real normalized yield, \hat{p}/O_{\odot} , unchanged with respect to a value deduced from an acceptable fit to the EGD in the disk solar neighbourhood (C00; C01). More precisely, about 80-90% of the initial halo gas has to be inhibited from forming stars and, on the other hand, about 10-50% of the initial bulge mass has to be added as gas enhanced in forming stars, for

providing an acceptable fit to the related EGD. It results in a normalized effective yield lower by about one order of magnitude in the halo, with respect to the bulge.

The TGD deduced from models H1-H2 and B1-B2 is represented in Fig. 6 and compared to the corresponding EGD in connection with halo (top panels) and bulge (bottom panels) field stars, both in presence (left panels) and in absence (right panels) of [O/Fe] plateau.

With regard to the halo, homogeneous simple models in presence of star formation inhibiting gas, provide an acceptable fit with values of input parameters as listed in Tab. 7 and $0.092 < \hat{p}''/O_{\odot} < 0.134$, both in presence and in absence of [O/Fe] plateau.

With regard to the bulge, homogeneous simple models in presence of star formation enhancing gas, provide an acceptable fit with values of input parameters as listed in Tab. 7 and $0.81 < \hat{p}''/O_{\odot} < 1.09$, both in presence and in absence of [O/Fe] plateau.

Further inspection of Fig. 6 shows that, in both cases, there is a slight deficiency (strengthened in absence of [O/Fe] plateau), in the number of stars observed below a threshold, $\phi \approx 0.004$ or $[\text{Fe}/\text{H}] \approx -3.0$ with regard to the halo, and $\phi \approx 0.5$ or $[\text{Fe}/\text{H}] \approx -0.6$ with regard to the bulge. In other words, a G-dwarf problem seems to exist for both the halo (Hartwick 1976; Prantzos 2003) and the bulge (Ferrerias et al. 2003).

The TGD deduced from models H1-H2 and B1-B2 is represented in Fig 7 and compared to the corresponding EGD in connection with the complete sample ($N = 149$) of globular clusters considered above (top panels), and a reduced sample ($N = 107$) with only old halo and bulge/disk objects retained (bottom panels), both in presence (left panels) and in absence (right panels) of [O/Fe] plateau. With regard to halo clusters, homogeneous simple models with star formation inhibiting gas, provide an acceptable fit leaving aside the occurrence of a G-dwarf problem. Accordingly, field halo stars and halo globular clusters underwent similar chemical evolution, which is consistent with recent results on the comparison of elemental abundance ratios (Pritzl, Venn & Irwin 2005).

With regard to bulge/disk clusters, homogeneous simple models with star formation enhancing gas, provide an acceptable fit below a threshold in metal abundance, $\phi \approx 0.6$ or $[\text{Fe}/\text{H}] \approx 0.5$, while a G-dwarf problem appears when the threshold is exceeded. On the other hand, it is not the case for bulge field stars, which implies that the formation of bulge/disk metal-rich globular

clusters was inhibited (in the sense that proto-cluster stars turned into field stars) and/or tidal disruption took place. Accordingly, bulge (and possibly thick disk) field stars and bulge/disk globular clusters underwent similar chemical evolution.

Clusters within a restricted metallicity range, $-1.2 \lesssim [\text{Fe}/\text{H}] \lesssim -0.8$, are fitted by both halo and bulge models, which allows to shift on the left the transition from halo to bulge/disk, from $[\text{Fe}/\text{H}] \approx -0.8$ to $[\text{Fe}/\text{H}] \approx -1.2$, consistent with a restricted range in age shown by metal-rich clusters, $[\text{Fe}/\text{H}] \gtrsim -1.0$, see Fig. 1.

With regard to Galactic spheroid field stars, the differential version of Eq. (13a) reads:

$$\begin{aligned} \psi &= \log \frac{dN}{N d\phi} = \log \frac{dN_H + dN_B}{N d\phi} \\ &= \log \left[\frac{N_H}{N} \frac{dN_H}{N_H d\phi} + \frac{N_B}{N} \frac{dN_B}{N_B d\phi} \right] ; \end{aligned} \quad (26a)$$

$$N_H = N_{FH} + (N_{GC})_H ; \quad N_B = N_{FB} + (N_{GC})_B ; \quad (26b)$$

which includes the contribution from globular clusters. The combination of Eqs. (10), (14), and (26) yields:

$$\psi = \log \left[\frac{M_H}{M} \exp_{10}(a_H \phi + b_H) + \frac{M_B}{M} \exp_{10}(a_B \phi + b_B) \right] ; \quad (27)$$

where, in general, $\exp_u x = x^u$ and $\exp_e x = e^x$ according to the usual notation. Then the TGD related to the Galactic spheroid is expressed by Eq. (27).

Two alternatives shall be considered, S_1 and S_2 , according if the coefficients, a and b , are taken from cases H1, B1, and H2, B2, of Tab. 8, respectively, and $M_H/M = 0.1$, $M_B/M = 0.9$, are assumed to a good extent. The resulting TGD is plotted in Fig. 8 and compared to its empirical counterpart, represented in Fig. 5 (bottom panels), both in presence (left panels) and in absence (right panels) of $[\text{O}/\text{Fe}]$ plateau. A discontinuity is exhibited by the TGD at $\phi = 0.20$, where bulge formation is assumed to start. Though a G-dwarf problem seems to exist for both the halo and bulge, the current model provides a viable interpretation to the occurrence of three extremum points, two maxima and one minimum, in the EGD.

5 Inhomogeneous, simple models

As a viable alternative to homogeneous simple models, let us take into consideration inhomogeneous simple models already used in previous approaches (C00; C01). In this view, the proto-halo/proto-bulge is conceived as structured into a number of discrete, entirely gaseous, identical regions, and a subsystem of long-lived stars, remnants, and star formation inhibiting gas, which have been generated earlier. The evolution occurs via a sequence of identical time steps. At the beginning of a step, star formation stochastically takes place in a subclass of “active” regions, as described by simple homogeneous models, while the others remain “quiescent”. At the end of a step, high-mass stars have died whereas low-mass stars have survived upto today, according to instantaneous recycling approximation. In addition, the enriched gas left from active regions is instantaneously mixed with the un-enriched gas within quiescent regions, to form a new set of identical regions for the next step. For further details, see C00.

The gas oxygen abundance, averaged over the whole system, still shows a monotonic increase with time, and depends on the gas mass fraction, according to Eq. (17), provided the fraction of active regions equals the probability of a region to be active (expected evolution; for further details, see C00). Taking into consideration also star formation inhibiting or enhancing gas, the effective yield takes the expression (C01):

$$\hat{p}' = \hat{p}'' \frac{(1-q)\mu'_R \ln \mu'_R}{(1-\mu'_R)q \ln q} ; \quad \hat{p}' \leq \hat{p}'' ; \quad (28)$$

$$q = 1 - \chi(1 - \mu'_R) ; \quad 0 \leq q \leq 1 ; \quad (29)$$

concerning an active region, \hat{p}'' is the effective yield due to star formation inhibiting or enhancing gas, expressed by Eq. (18), and μ'_R the gas mass fraction at the end of a step; concerning the system, q may be thought of as an effective gas mass fraction within a region at the end of a step, i.e. the mean gas mass fraction averaged on both active and quiescent regions, and χ is the probability of a region being active at the beginning of a step. For further details, see C00.

Though the TGD cannot be analytically expressed in the framework of inhomogeneous simple models, still it can be done in the special case of expected evolution, with regard to the starting point, $\psi(\phi_o) = \psi_o$, and the

ending point of the initial step, $\psi(\phi_o + \Delta\phi_o) = \psi_1$, where $\Delta\phi_o$ is the net oxygen abundance (normalized to the solar value) increase in gas component at the end of the first step. The result is (C01):

$$\psi_o = \psi(\phi_o) = \log \left[\frac{1}{N} \left(\frac{dN}{d\phi} \right)_{\phi_o} \right] = \log \left(\frac{\chi\mu_o}{\mu_o - \mu_f} \frac{O_\odot}{\hat{p}''} \right) ; \quad (30)$$

$$\begin{aligned} \psi_1 &= \psi(\phi_o + \Delta\phi_o) = \log \left[\frac{1}{N} \frac{\Delta N_o}{\Delta\phi_o} \right] \\ &= \log \left\{ \frac{1}{\Delta\phi} \left[1 - \exp \left(-\frac{\Delta\phi}{\hat{p}} O_\odot \right) \right] \right\} + \log \frac{\chi\mu_o}{\mu_o - \mu_f} ; \end{aligned} \quad (31)$$

where ΔN_o is the number of stars belonging to a selected spectral class, within the oxygen abundance range, $\phi_o \leq \phi \leq \phi_o + \Delta\phi_o$, and $\Delta\phi_o = \Delta\phi$ independent of the step, in the case under discussion of expected evolution.

An approximate expression of the TGD related to the first step, ψ_1 , with the terms up to the second order retained, reads (C01):

$$\psi_1 = \psi(\phi_o + \Delta\phi_o) = -\frac{1}{\ln 10} \frac{O_\odot}{\hat{p}''} \frac{\Delta\phi}{2} + \log \left(\frac{\chi\mu_o}{\mu_o - \mu_f} \frac{O_\odot}{\hat{p}''} \right) ; \quad \frac{O_\odot}{\hat{p}''} \frac{\Delta\phi}{2} \ll 1 ; \quad (32)$$

which is valid also in the general case, provided $\Delta\phi$ is replaced by $\Delta\phi_o$ and the probability, χ , by the relative frequency, $\nu_o = k_o/n_o$, being k_o and n_o the number of active and all regions, respectively, with regard to the first step.

The values of some parameters related to the expected evolution, concerning cases H1, H2, B1, B2, are listed in Tab.9. The parameters appearing therein, which equal their counterparts corresponding to homogeneous models (Tabs. 7 and 8), must be connected with active regions, and for this reason some corresponding output parameters show different values. For further details, see Appendix A. New input parameters are: the effective yield, \hat{p}' , and the normalized oxygen abundance increase at the end of a step with regard to the whole system, $\Delta\phi$, and to an active region, $\Delta\phi'_R$, respectively.

Concerning an active region, parameter values at the end of a step are calculated using a homogeneous simple model with star formation inhibiting or enhancing gas. Let μ'_R , s'_R , and D'_R , be related to star formation allowing gas, long-lived stars, and star formation inhibiting or enhancing gas, from or enhanced in forming stars, respectively. Taking star formation inhibiting gas and leaving other parameters unchanged, makes no variation in the final gas

Table 9: Values of parameters related to the expected evolution of inhomogeneous simple models, in connection with two different cases for the halo, H1 and H2, and for the bulge, B1 and B2, respectively. The indices, 2.9 and 2.35, denote values related to the power-law IMF exponent, p , in computing the corresponding quantities. With regard to the parameter, ψ_1 , upper and lower values are calculated by use of Eqs. (31) and (32), respectively. The effective yield, \hat{p}' , is related to inhomogeneities in oxygen abundance due to the presence of active and quiescent regions, whereas oxygen is uniformly distributed within active regions. The lower part of the table is related to models with star formation inhibiting or enhancing gas. Parameters not reported therein have same value as in the upper part, with the exception of \hat{p} , α , and m_{mf} , which are listed in Tab. 7 together with other parameters not appearing here. The effective yield, \hat{p}'' , related to star formation inhibiting or enhancing gas, is listed as \hat{p} in the upper part of the table. The effective yield, \hat{p}' , due to the presence of both star formation inhibiting or enhancing gas within active regions, and star formation precluding gas within quiescent regions, is listed with the same notation in the upper part of the table. The index, R , denotes a generic active region. The mean oxygen abundance (normalized to the solar value) of stars at the end of evolution is denoted as $\bar{\phi}$. Positive and negative κ - D values correspond to star formation inhibiting and enhancing gas, respectively. Mass fractions are normalized to the initial mass.

	H1	H2	B1	B2
μ'_R	8.2201 E-4	4.0337 E-5	1.4139 E-1	8.5397 E-2
q	4.4991 E-2	1.7298 E-3	2.4833 E-1	1.4548 E-1
κ	9.5579 E-1	9.9831 E-1	8.7545 E-1	9.3431 E-1
\hat{p}/O_\odot	1.3363 E-1	9.2288 E-2	1.0857 E-0	8.1430 E-1
\hat{p}'/O_\odot	5.3452 E-3	3.4180 E-3	7.6001 E-1	5.7001 E-1
μ_f	4.0973 E-6	8.9544 E-5	3.8030 E-3	4.4794 E-4
$\alpha_{2.9}$	9.3914 E-1	9.5717 E-1	6.5510 E-1	7.1692 E-1
$\alpha_{2.35}$	9.7832 E-1	9.8492 E-1	8.4739 E-1	8.8101 E-1
$(\tilde{m}_{mf})_{2.9}$	6.7781 E-2	4.5917 E-2	4.6050 E-1	3.7068 E-1
$(\tilde{m}_{mf})_{2.35}$	7.5651 E-5	2.6985 E-5	1.7263 E-2	8.7958 E-3
$\Delta\phi$	1.6577 E-2	2.1738 E-2	1.0587 E-0	1.0988 E-0
$\Delta\phi'_R$	9.4927 E-1	9.3379 E-1	2.1239 E-0	2.0035 E-0
ψ_o	8.5446 E-1	1.0341 E-0	-9.1837 E-2	5.9898 E-2
$\psi_1(31)$	8.2781 E-1	9.8398 E-1	-2.8650 E-1	-2.0066 E-1
$\psi_1(32)$	8.2753 E-1	9.8297 E-1	-3.0358 E-1	-2.3312 E-1
κ	4.5169 E-0	6.9883 E-0	-3.2093 E-1	-9.4658 E-2
s'_R	1.8111 E-1	1.2518 E-1	1.2645 E-0	1.0102 E-0
D'_R	8.1807 E-1	8.7478 E-1	-4.0590 E-1	-9.5626 E-2
$\bar{\phi}$	1.3385 E-1	9.3250 E-2	9.3597 E-1	8.2723 E-1
s_f	1.8126 E-1	1.2518 E-1	1.4671 E-0	1.1041 E-0
D_o	8.1874 E-1	8.7482 E-1	-4.7094 E-1	-1.0451 E-1

mass fraction, μ_f , as it is irrelevant if gas is frozen into long-lived stars or inhibited from forming stars. Accordingly, the final star plus star formation inhibiting or enhancing gas mass fraction, $s_f + D_f = 1 - \mu_f$, also remains unchanged. On the other hand, $s'_R + D'_R = 1 - \mu'_R$ within active regions at the end of a step, where $s'_R/D'_R = s_f/D_f$ necessarily holds. The combination of the above relations yields:

$$s_f = \frac{1 - \mu_f}{1 - \mu'_R} s'_R ; \quad (33)$$

$$D_f = \frac{1 - \mu_f}{1 - \mu'_R} D'_R ; \quad (34)$$

which are listed in the lower part of Tab. 9.

The TGD related to cases H1, B1, (full lines) and H2, B2, (dashed lines) is compared in Fig. 9 to the corresponding EGD with regard to halo (top panels) and bulge (bottom panels) field stars, both in presence (left panels) and in absence (right panels) of [O/Fe] plateau.

With regard to the halo, inhomogeneous simple models with star formation inhibiting gas, provide an acceptable fit using values of input parameters listed in Tab. 7 and $0.0033 < \hat{p}'/O_\odot < 0.0054$, in presence and/or in absence of [O/Fe] plateau.

With regard to the bulge, inhomogeneous simple models with star formation enhancing gas, provide an acceptable fit using values of input parameters listed in Tab. 7 and $0.56 < \hat{p}'/O_\odot < 0.77$, in presence and/or in absence of [O/Fe] plateau.

In dealing with active regions, the normalized oxygen abundance at the end of evolution, ϕ_f , has to be replaced with the normalized oxygen abundance at the end of a step, $\phi_i + \Delta\phi'_R$.

Further inspection of Fig. 9 shows that, with respect to homogeneous simple models plotted in Fig. 6, the fit is more or less unchanged for the halo, and slightly improved for the bulge. In any case, a G-dwarf problem still remains.

The TGD related to cases H1, B1, (full lines) and H2, B2, (dashed lines) is compared in Fig. 10 to the corresponding EGD with regard to the whole sample ($N = 149$) of globular clusters considered above (top panels), and a reduced sample ($N = 107$) of old halo and bulge/disk objects (bottom panels), both in presence (left panels) and in absence (right panels) of [O/Fe]

plateau. The trend looks like its counterpart exhibited by homogeneous simple models, and similar considerations can be made.

The TGD related to the Galactic spheroid has to be numerically computed using Eq. (26) together with H1, B1; H2, B2; models listed in Tab. 9, yielding cases S1, S2, respectively. Fractional masses equal to $M_H/M = 0.1$, $M_B/M = 0.9$, have been assumed to a good extent. A comparison with the related EGD (Fig. 5, bottom panels) is made in Fig. 11 both in presence (left panels) and in absence (right panels) of [O/Fe] plateau. The trend looks like its counterpart exhibited by homogeneous simple models, and similar considerations can be made.

The temporal behaviour of (allowing star formation) gas oxygen abundance (TAMR), normalized to the solar value, $\log \phi = [\text{O}/\text{H}]$, related to models H1 and B1, are plotted in Figs. 12 and 13, in presence and in absence of [O/Fe] plateau, respectively. Also plotted therein are the data coming from a sample of 55 Galactic globular clusters (De Angeli et al. 2005) but expressed in terms of absolute ages (De Angeli 2005), with same captions as in Fig. 1. The conversion from [Fe/H] to [O/H] has been made using Eqs. (1) and (2) in presence and in absence of [O/Fe] plateau, respectively. It is worth recalling that simple models of chemical evolution used in the current paper are time independent, with regard to the TGD. Accordingly, the initial and the final time, together with the time step in the case of inhomogeneous models, can be selected for best fitting the empirical age-metallicity relation (EAMR).

With regard to the halo, initial and final values, $([\text{O}/\text{H}], T/\text{Gyr}) = (-3, 12.5)$ and $(0, 8.0)$, respectively, have been chosen, together with a time step, $\Delta T/\text{Gyr} = 1.125$, for a total of four. The related TAMR is represented by four full curves in Figs. 12 and 13.

With regard to the bulge, initial and final values, $([\text{O}/\text{H}], T/\text{Gyr}) = (-0.70, 10.5)$ and $(0.74, 10.0)$, respectively, have been chosen, together with a time step, $\Delta T/\text{Gyr} = 0.125$, for a total of four. The related TAMR is represented by a single full curve in Figs. 12 and 13, the remaining three being out of scale on the right.

The comparison between EAMR (related to globular clusters) and TAMR (related to both globular clusters and field stars) shows that surviving (or formed) halo globular clusters belong to all model time steps, while surviving (or formed) bulge/disk globular clusters belong to the first step only and, in fact, are coeval within the age uncertainties.

In the framework of inhomogeneous models, star formation allowing gas

has to be able of generating both active and quiescent regions. With regard to models H and B listed in Tab. 9, almost all star formation allowing gas has been exhausted at the end of evolution, leaving about 18-13% of long-lived stars and 82-87% of star formation inhibiting gas in the halo, and about 72-91% of long-lived stars from primeval gas and 28-9% from inflowing gas in the bulge, related to the final mass. The mean normalized oxygen abundance within stars is about 0.13-0.093 and 0.94-0.83 in the halo and the bulge, respectively. It is worth of note that the Galactic spheroid (halo and bulge) would be mostly luminous for a IMF exponent, $p = 2.9$, and mostly dark for $p = 2.35$, owing to different lower stellar mass limits, by more than an order of magnitude. On the other hand, the assumption of a universal IMF implies the same yield, and lower stellar mass limit, for the spheroid and the disk.

The comparison between homogeneous (Tab. 8) and inhomogeneous (Tab. 9) simple models, shows no substantial change in TGD. It is worth emphasizing that the only difference is in the physical process related to the effective yield, which is due to star formation inhibiting or enhancing gas for homogeneous models and, in addition, to the presence of active and quiescent regions for inhomogeneous models. On the other hand, the related TAMR cannot provide an acceptable fit in the former alternative, but can do in the latter, as shown in Figs. 12 and 13.

6 Discussion

According to the results of Sections 3 and 4, halo and bulge EGD, taken separately, are consistent with both homogeneous (Fig. 6) and inhomogeneous (Fig. 9) simple models of chemical evolution. The former alternative has been widely discussed (e.g., Hartwick 1976; Caimmi 1981, 1982; Ryan & Norris 1991). The latter one allows a direct comparison with its counterpart related to the disk solar neighbourhood (C00), under the assumption of a universal, power-law IMF.

As regards the disk solar neighbourhood, a lower stellar mass limit, exceeding the theoretical Jeans stellar mass ($0.007 \leq \tilde{m}_J \leq 0.01$), occurs for a power-law exponent $p = -2.9$, which is a fit to the Scalo (1986) IMF for $m \gtrsim m_\odot$, concerning both mass distribution and oxygen production (Wang & Silk 1993). A less steep Salpeter (1955) IMF, implying $p = -2.35$, is marginally consistent with the theoretical Jeans stellar mass (Tab. 7). On

Table 10: Comparison between parameters of inhomogeneous simple models, related to halo and bulge (cases H1 and B1 of Tab.9) and disk solar neighbourhood (C01, Tab.5). An universal power-law initial mass function (IMF) is assumed in all cases, which leaves other parameters i.e. \hat{p} , α , and m_{mf} , unchanged. Gas and star mass fractions, μ_f , D_f , and s_f , are related to the initial mass with regard to the bulge, where total mass conservation is violated by gas inflow.

meaning	parameter	value		
		halo	bulge	disk
probability	χ	$9.5579 \cdot 10^{-1}$	$8.7545 \cdot 10^{-1}$	$7.6765 \cdot 10^{-2}$
gas mass fraction	μ'_R	$8.2201 \cdot 10^{-4}$	$1.4139 \cdot 10^{-1}$	$3.7148 \cdot 10^{-1}$
gas mass fraction	q	$4.4991 \cdot 10^{-2}$	$2.4833 \cdot 10^{-1}$	$9.5175 \cdot 10^{-1}$
inhibition parameter	κ	4.5169	$-3.2099 \cdot 10^{-1}$	0.0000
gas mass fraction	μ_f	$4.0973 \cdot 10^{-6}$	$3.8030 \cdot 10^{-3}$	$2.9047 \cdot 10^{-1}$
gas mass fraction	D_f	$8.1874 \cdot 10^{-1}$	$-4.7094 \cdot 10^{-1}$	0.0000
star mass fraction	s_f	$1.8126 \cdot 10^{-1}$	1.4671	$7.0953 \cdot 10^{-1}$
normalized yield	\hat{p}''/O_\odot	$1.3363 \cdot 10^{-1}$	$7.6001 \cdot 10^{-1}$	$7.3722 \cdot 10^{-1}$
normalized yield	\hat{p}'/O_\odot	$5.3452 \cdot 10^{-3}$	1.0857	$4.4233 \cdot 10^{-1}$

the other hand, the occurrence of stellar wind would reduce oxygen nucleosynthesis by a factor of about 2.5 (e.g., Wang & Silk 1993) which, in turn, would raise the lower stellar mass limit (e.g., C01).

The more relevant parameters of inhomogeneous simple models related to halo, bulge, and disk solar neighbourhood, are listed in Tab.10. The related values are taken from Tab.9 (models H1 and B1) and C01 (Tab.5), respectively. An universal power-law IMF is assumed, $\phi(\tilde{m}) \propto \tilde{m}^{-p}$, which makes no change in value of the physical parameters, \hat{p} , α , and m_{mf} .

With regard to active regions, the probability of star formation is $\chi \lesssim 1$ for the halo, $\chi < 1$ for the bulge, and $\chi \ll 1$ for the disk. Accordingly, the gas mass fraction left at the end of a step, μ'_R , is close to zero for the halo, about one seventh for the bulge, and about one third for the disk. The effective yield, \hat{p}'' , is about six times larger in the disk (where it coincides

with the real yield) and in the bulge (where star formation is enhanced by inflowing gas with same composition as in the pre-existing gas), than in the halo (where gas is partially inhibited from forming stars).

With regard to the whole system, a similar trend occurs. The ratio of gas mass fraction at the end and at the beginning of a step is $q \ll 1$ for the halo, $q < 1$ for the bulge, and $q \lesssim 1$ for the disk. Accordingly, the (allowing star formation) gas mass fraction left at the end of evolution, μ_f , is close to zero for the halo and about four thousandths for the bulge, and about one third for the disk. The effective yield, \hat{p}' , is about one half thousand times larger in the bulge (where it is due to both inhomogeneous star formation and gas inflow), and about one thousand times larger in the disk (where it is due to inhomogeneous star formation) than in the halo (where it is due to both inhomogeneous star formation and inhibition from forming stars). With regard to the total mass at the end of evolution, it is left about 18% of long-lived stars (including remnants) and 84% of gas inhibited from forming stars in the halo; about 72% of long-lived stars from primeval gas and 28% from inflowed gas in the bulge; about 71% of long-lived stars and 29% of gas allowing star formation in the disk.

The TGD related to both homogeneous and inhomogeneous simple models provides an acceptable fit to the EGD related to the Galactic spheroid (Figs.8 and 11) and, in particular, a non monotonic trend is reproduced. While models assume that star formation at the beginning of halo and bulge evolution starts abruptly with constant efficiency, the data seem to indicate a somewhat gradual rate, with increasing efficiency. In other words, the occurrence of some physical process (not necessarily gas infall) seems to inhibit halo and bulge star formation in early times. Accordingly, the history of each Galactic subsystem (halo, bulge, disk) could be conceived as made of two distinct phases, namely (i) assembling, where star formation efficiency is gradually increasing, and (ii) stabilization, where star formation efficiency maintains constant.

At the end of halo evolution, the fractional gas and star mass predicted by the model, are:

$$\frac{M_{H \text{ gas}}}{M_{Ho}} = \mu_f + D_f \quad ; \quad (35)$$

$$\frac{M_{H \text{ stars}}}{M_{Ho}} = s_f \quad ; \quad (36)$$

where M_{Ho} is the initial halo mass. The combination of Eqs. (35) and (36) yields:

$$M_{H \text{ gas}} = \frac{\mu_f + D_f}{s_f} M_{H \text{ stars}} ; \quad (37)$$

where $M_{H \text{ stars}}$ is the current halo mass.

At the end of bulge evolution, the fractional gas plus stars and star mass due to gas inflow, predicted by the model, are:

$$\frac{M_{B \text{ stars}} + M_{B \text{ gas}}}{M_{Bo}} = \mu_f + s_f ; \quad (38)$$

$$\frac{M_{B \text{ stars}}^-}{M_{Bo}} = -D_f ; \quad (39)$$

where M_{Bo} is the initial bulge mass and $M_{B \text{ stars}}^-$ is the star mass due to gas inflow, at the end of evolution. The combination of Eqs. (38) and (39) yields:

$$M_{B \text{ stars}}^- = \frac{-D_f}{\mu_f + s_f} (M_{B \text{ stars}} + M_{B \text{ gas}}) ; \quad (40)$$

where $M_{B \text{ stars}} + M_{B \text{ gas}}$ is the current bulge mass.

With regard to models H1-2, B1-2, the values of fractional masses, μ_f , s_f , D_f , are listed in Tab. 9, and taking a current halo mass $M_H = M_{H \text{ stars}} = 10^9 m_\odot$ and a current bulge mass $M_H = M_{B \text{ stars}} + M_{B \text{ gas}} = 10^{10} m_\odot$, it is found the following:

$$M_{H \text{ gas}} = 4.5-7.0 \cdot 10^9 m_\odot ; \quad (41)$$

$$M_{B \text{ stars}}^- = 3.2-0.95 \cdot 10^9 m_\odot ; \quad (42)$$

which is in agreement with the idea, that a fraction of the current bulge mass inflowed from the halo. The disk might have evolved separately for two orders of reasons.

First, the empirical distribution of angular momentum in halo, bulge, thick disk, and thin disk stars seems to be consistent with a decoupled dynamical evolution of the halo and the thick disk i.e. dissipative halo-bulge and thick disk-thin disk collapse (Wyse & Gilmore 1992; Ibata & Gilmore 1995). Accordingly, the chemical evolution of the above mentioned subsystems could also have been decoupled.

Second, the disk mass (gas + stars) is estimated as $M_D = M_{D\text{stars}} + M_{D\text{gas}} \approx (5.0 + 0.8)10^{10}m_\odot = 5.8 \cdot 10^{10}m_\odot$ (e.g., Prantzos & Silk 1988), which cannot be provided by outflowing halo gas for more than about one tenth of the above value, according to Eqs. (41) and (42).

On the other hand, a continuous transition seems to exist from an extended ($R \gtrsim 20$ kpc), pressure-supported halo, to an inner, flattened ($R \lesssim 15$ kpc), rotation-supported halo (Chiba & Beers 2000). In addition, no correlation appears between mean rotational velocity and metal abundance for values below $[\text{Fe}/\text{H}] \approx -1.7$ or $\phi \approx 0.08$, whereas exhibits a linear trend for larger values. The mean rotational velocity exceeds the statistical fluctuations related to metal-poor stars from $[\text{Fe}/\text{H}] \approx -1.3$ or $\phi \approx 0.2$ on, and the relative abundance of thick disk stars is less than 1% for $[\text{Fe}/\text{H}] \approx -1.7$. For further details, see Chiba & Beers (2000). It is worth noticing that the range, $-1.7 \lesssim [\text{Fe}/\text{H}] \lesssim -1.3$, with regard to ZW metallicity scale, is related to a larger age spread in globular clusters, as shown in Fig. 1.

The chemical abundance of thick disk stars suggests a similar history to those of metal-rich ($[\text{Fe}/\text{H}] \approx -1.3$) halo stars (Prochaska et al. 2000). In addition, the thick disk abundance patterns show excellent agreement with the chemical abundances observed in metal-poor bulge stars, suggesting the two populations were formed from the same gas reservoir at a common epoch. For further details, see Prochaska et al. (2000).

To include the disk in a qualitative discussion, let us assume that a baryonic dark halo exists, or an equivalent mass was lost during bulge and disk formation (C01). Accordingly, the following relations hold:

$$\frac{M_I}{M} = \frac{M_I}{M_{\text{vis}}} \frac{M_{\text{vis}}}{M}; \quad I = H, B, D; \quad (43a)$$

$$M_{\text{vis}} = M_H + M_B + M_D; \quad (43b)$$

$$M = M_{\text{vis}} + M_{\text{uns}}; \quad (43c)$$

and, in addition:

$$\frac{M_H + M_{\text{uns}}}{M} = \frac{M_{\text{stars}}}{M}; \quad \frac{M_B + M_D}{M} = \frac{M_{\text{gas}}}{M}; \quad (44)$$

where M_{vis} is the visible Galactic mass, M_{uns} the unseen (baryonic) mass, and $M_H + M_{\text{uns}}$ is the total halo mass, including the baryonic dark subsystem or the lost mass.

Using the above quoted values for M_H , M_B , M_D , it is found $M_H/M_{\text{vis}} = 0.01449$, $M_B/M_{\text{vis}} = 0.14493$, $M_D/M_{\text{vis}} = 0.84058$, and $M_{\text{vis}} = 6.9 \cdot 10^{10} m_{\odot}$. On the other hand, the values of fractional masses, μ_f , s_f , and D_f , predicted by the model, must be related to the total mass, M . Accordingly, the following relation holds:

$$\frac{M_B + M_D}{M_{\text{vis}}} = 0.98551 \quad ; \quad (45)$$

via Eq. (44), and:

$$\frac{M_{H \text{ gas}}}{M} = \mu_f + D_f \quad ; \quad (46)$$

as predicted by the model via Eq. (35), provided the initial halo mass coincides with the initial Galactic mass. If, in addition, bulge and (thick) disk formation took place from the same gas reservoir, as suggested by observations (Prochaska et al. 2000), it may safely be assumed that the proto-halo was the common reservoir, which implies Eq. (44).

The combination of Eqs. (43a), (44), and (46) yields:

$$\frac{M_B + M_D}{M_{\text{vis}}} \frac{M_{\text{vis}}}{M} = \mu_f + D_f \quad ; \quad (47)$$

where the mass fractions, μ_f and D_f , are listed in Tab.9 with regard to models H1 and H2. Using Eqs. (43) and (45), the following mass ratios are determined:

$$\frac{M_{\text{vis}}}{M} = 0.83078 - 0.88768 \quad ; \quad (48a)$$

$$\frac{M_{\text{uns}}}{M} = 0.16922 - 0.11232 \quad ; \quad (48b)$$

$$\frac{M_H}{M} = 0.012040 - 0.012865 \quad ; \quad (48c)$$

$$\frac{M_B}{M} = 0.12040 - 0.12865 \quad ; \quad (48d)$$

$$\frac{M_D}{M} = 0.69834 - 0.74618 \quad ; \quad (48e)$$

$$\frac{M_H}{M_{\text{uns}}} = 0.071150 - 0.11454 \quad ; \quad (48f)$$

which shows that the unseen (baryonic) halo, or the total amount of gas lost, has to be as massive as about the bulge.

In the light of the current model, it is apparent that about 17%-11% of the total mass gave no contribution to bulge and disk formation. If this material is related to stars with a mass below a threshold, m_0 , then the mass ratio of long-lived stars above and below the threshold must necessarily equal the mass ratio, M_H/M_{uns} . The further restriction to a power-law IMF, $\phi(\tilde{m}) \propto \tilde{m}^{-p}$, implies the validity of the relation (C01):

$$\frac{\tilde{m}_{mr}^{2-p} - \tilde{m}_o^{2-p}}{\tilde{m}_o^{2-p} - \tilde{m}_{mf}^{2-p}} = \frac{M_H}{M_{\text{uns}}} ; \quad \tilde{m} = \frac{m}{m_\odot} ; \quad (49)$$

where m_{mr} is the mass of the oldest halo stars which are currently leaving the main sequence. For a model halo formation from 12.5 to 8.0 Gyr ago, $m_{mr} = 0.9 m_\odot$ is expected to be consistent with the theory of stellar evolution. In fact, a value $m_{mr} = 0.87 m_\odot$ is deduced by linear interpolation from results related to metal-free stars (Marigo et al. 2001), and the above value has to be raised due to the observational lack of halo stars with zero metallicity.

Taking $\tilde{m}_{mr} = 0.9$, \tilde{m}_{mf} from Tab. 7, and using Eq. (48f), the threshold mass, \tilde{m}_o , may be deduced from Eq. (49). The result is:

$$\tilde{m}_o = 0.25048 - 0.26178 ; \quad p = 2.9 ; \quad (50a)$$

$$\tilde{m}_o = 0.089514 - 0.10027 ; \quad p = 2.35 ; \quad (50b)$$

accordingly, stars with lower mass (for fixed power-law IMF exponent, p) either escaped detection up today, or became unbound to the halo.

If, on the other hand, the unseen baryonic halo is gaseous and unbound to the Galaxy, the power-law IMF exponent related to $\tilde{m}_{mf} = \tilde{m}_o$, leaving the remaining input parameters unchanged, reads:

$$p = 2.8089 - 2.8206 ; \quad (51a)$$

$$p = 2.6025 - 2.6205 ; \quad (51b)$$

related to Eqs. (50a) and (50b), respectively. Accordingly, the values $p = 2.9$ and $p = 2.35$ may be regarded as fiducial limiting values.

An alternative explanation demands a different IMF in different Galactic subsystems. A minor change could only occur in the lower stellar mass limit, owing to a larger Jeans stellar mass (e.g., Larson 1998). Accordingly, a gas

amount prescribed to form stars in the range below the Jeans stellar mass, $\tilde{m}_{mf} \leq \tilde{m} \leq \tilde{m}_o$, would follow a different fate, being lost from the system (e.g., Binney et al. 2001). The inhibition of star formation in the mass range under discussion, could be due, in addition, to less efficient cooling in metal-poor proto-stars. In fact, the pre-main sequence life time would be increased, to exceed the main sequence life time of massive stars. Finally, low-mass proto-stars would be destroyed by supernovae and the related gas, which is expected to be weakly bound to the proto-Galaxy, would be lost during bulge and disk formation.

7 Conclusion

The empirical differential oxygen abundance distribution (EGD) in the Galactic spheroid has been deduced from three different samples involving (i) 268 K-giant bulge stars (Sadler et al. 1996), and (ii) 149 globular clusters (Mackey & van den Bergh 2005) for which the iron abundance distribution is known, in addition to previous results (Caimmi 2001) related to (iii) 372 solar neighbourhood halo subdwarfs (Ryan & Norris 1991). To this aim, two alternative $[\text{O}/\text{H}]$ - $[\text{Fe}/\text{H}]$ dependences have been used, according to Eqs. (1) and (2), respectively. The data have been fitted, to an acceptable extent, by both homogeneous and inhomogeneous simple models of chemical evolution.

Under the assumption of a universal initial mass function (IMF) and same value of the true yield as in the disk solar neighbourhood, inhibition of halo star formation (implying gas outflow) and enhancement of bulge star formation (implying gas inflow) have been demanded for fitting the EGD. On the contrary, no such gas outflow or inflow was requested to reproduce the EGD in the disk solar neighbourhood (C00). A power-law IMF has been considered, $\phi(\tilde{m}) \propto \tilde{m}^{-p}$, within the range, $2.35 \leq p \leq 2.9$, and special effort has been devoted to the limiting cases, $p = 2.9$, which is acceptably close to Scalo IMF for $m \gtrsim m_\odot$, and (ii) an exponent $p = 2.35$, which is the Salpeter IMF. In any case, it has been inferred that a more refined model involving an initially increasing star formation efficiency (but not necessarily implying gas infall) while assembling Galactic subsystems, could provide a better agreement with the data.

Homogeneous models have been recognized unable in fitting the empirical age-metallicity relation (EAMR) with regard to a homogeneous sample

of globular clusters De Angeli et al. 2005; De Angeli 2005), which shows a non monotonic trend characterized by large dispersion. On the other hand, inhomogeneous models have been shown an acceptable fit, provided globular cluster formation occurred through four different steps in the halo and through a single step in the bulge/disk, unless clusters of later generation were disrupted.

With regard to gas outflow from the halo, acceptable models made the following predictions. If spheroid and disk component underwent distinct evolutions, then a non negligible fraction of the bulge mass (from about one third to about one tenth) outflowed from the halo, for assumed $M_H = 10^9 m_\odot$ and $M_B = 10^{10} m_\odot$. If, on the other hand, spheroid and disk component underwent a common evolution, then an unseen baryonic halo (or equivalent amount of gas lost by the Galaxy) has been shown to be needed, for assumed $M_D = 5.810^{10} m_\odot$. The mass of the unseen halo has been found to be of the same order as the bulge mass. In addition, the treshold star mass below which the halo is not detectable (or the stars are unbound to the Galaxy) has been calculated as $m_o \approx 0.25 m_\odot$ for IMF exponent $p = 2.9$, and $m_o \approx 0.1 m_\odot$ for $p = 2.35$; conversely, $p \approx 2.8$ for lower stellar mass limit $m_{mf} = 0.25 m_\odot$, and $p \approx 2.6$ for $m_{mf} = 0.1 m_\odot$.

Acknowledgements

We thank F. De Angeli for making available values of absolute ages, errors, and additional data, related to the quoted reference De Angeli et al. (2005), and for stimulating e-mail correspondence. We also thank J. Fulbright and M. Rich for making available a preprint of the quoted reference Fulbright, McWilliam & Rich (2005) and, together with D. Terndrup, for fruitful e-mail correspondence.

Appendix

A Correspondence between homogeneous and inhomogeneous simple models

With regard to a generic system, let $\mu_o, \mu_f; \phi_o, \phi_f$; be initial and final values of fractional (allowing star formation) gas mass and oxygen abundance normalized to the solar value, respectively. Let chemical evolution be described using either homogeneous or inhomogeneous simple models. Finally, let the generalized yield, \hat{p}'' , related to the system in the former alternative, coincide with its counterpart related to an active region in the latter alternative.

With regard to a generic active region at the end of a step, Eq. (17) reduces to (C01):

$$\Delta\phi'_R = -\frac{\hat{p}''}{O_\odot} \ln \mu'_R \quad ; \quad (52)$$

where $\Delta\phi'_R = \phi'_{Rf} - \phi'_{Ro}$, $\mu'_{Ro} = 1$, and $\mu'_{Rf} = \mu'_R$. The combination of Eqs. (3), (17), and (52), in the case under discussion yields:

$$\frac{\phi_f - \phi_o}{\Delta\phi'_R} = \frac{\ln(\mu_f/\mu_o)}{\ln \mu'_R} \quad ; \quad (53)$$

which allows the calculation of the fractional gas mass ratio, μ_f/μ_o , predicted by homogeneous simple models, in terms of parameters related to inhomogeneous simple models with equal values of initial and final normalized oxygen abundance, ϕ_o , and ϕ_f , respectively.

With regard to homogeneous simple models, the mean normalized oxygen abundance in long-lived stars at the end of evolution is (C01, Appendix D):

$$\bar{\phi} = \bar{\phi}(\phi_f) = \phi_o + (\phi_f - \phi_o) \frac{u(1 - \ln u) - 1}{(1 - u) \ln u} \quad ; \quad u = \frac{\mu_f}{\mu_o} \quad ; \quad (54)$$

and the combination of Eqs. (3), (17), and (54) yields:

$$\bar{\phi}_f = \phi_o + \frac{\hat{p}''}{O_\odot} \left[1 + \frac{u \ln u}{1 - u} \right] \quad ; \quad u = \frac{\mu_f}{\mu_o} \quad ; \quad (55)$$

where $u = \mu_f$ in the special case, $\mu_o = 1$.

With regard to inhomogeneous simple models, the mean normalized oxygen abundance in long-lived stars at the end of the ℓ -th step is (C01, Appendix D):

$$\bar{\phi}_\ell = \frac{\sum_{i=0}^{\ell} \phi_i \nu_i \mu_i}{\sum_{i=0}^{\ell} \nu_i \mu_i} + \frac{\mu'_R (1 - \ln \mu'_R) - 1}{(1 - \mu'_R) \ln \mu'_R} \Delta \phi'_R ; \quad (56)$$

where ν_i is the relative frequency of active regions at the i -th step.

In the special case of expected evolution, $\nu_i = \chi$, the first term on the right-hand side of Eq. (56) reduces to (C01, Appendix D):

$$\frac{\sum_{i=0}^{\ell} \phi_i \nu_i \mu_i}{\sum_{i=0}^{\ell} \nu_i \mu_i} = \phi_0 - \frac{\hat{p}' q \ln q}{\text{O}_\odot (1 - q)} \left[1 - \frac{(\ell + 1) q^\ell (1 - q)}{1 - q^{\ell+1}} \right] ; \quad (57)$$

where \hat{p}' is the generalized yield related to the system, and q may be thought of as an effective gas mass fraction within a region at the end of a step i.e. the mean gas mass fraction averaged on both active and quiescent regions. The combination of Eqs. (28) and (57) yields:

$$\frac{\sum_{i=0}^{\ell} \phi_i \nu_i \mu_i}{\sum_{i=0}^{\ell} \nu_i \mu_i} = \phi_0 - \frac{\hat{p}'' \mu'_R \ln \mu'_R}{\text{O}_\odot (1 - \mu'_R)} \left[1 - \frac{(\ell + 1) q^\ell (1 - q)}{1 - q^{\ell+1}} \right] ; \quad (58)$$

in terms of the generalized yield, \hat{p}'' , related to an active region. The substitution of Eqs. (52) and (58) into (56) produces:

$$\bar{\phi}_\ell = \phi_0 + \frac{\hat{p}''}{\text{O}_\odot} \left[1 + \frac{\mu'_R \ln \mu'_R (\ell + 1) q^\ell (1 - q)}{1 - \mu'_R (1 - q^{\ell+1})} \right] ; \quad (59)$$

at the end of the ℓ -th step.

In the special case where the system reduces to a single region and the evolution to a single step, $\mu_f/\mu_o = \mu'_R$, $\ell = 0$, Eq. (59) reads:

$$\bar{\phi}_\ell = \phi_0 + \frac{\hat{p}''}{\text{O}_\odot} \left[1 + \frac{\mu'_R \ln \mu'_R}{1 - \mu'_R} \right] ; \quad (60)$$

which coincides with Eq. (55), related to homogeneous simple models.

The above results may be reduced to a single statement.

Theorem Given (i) an inhomogeneous simple model of chemical evolution with assigned values of initial normalized oxygen abundance, ϕ_o , generalized

yield related to an active region, \hat{p}'' , and gas mass fraction within an active region at the end of a step, μ'_R ; and (ii) a homogeneous simple model of chemical evolution with initial normalized oxygen abundance, ϕ_o , generalized yield related to the system, \hat{p}'' , and gas mass fraction at the end of evolution, $\mu_f = \mu'_R$; the mean oxygen abundance in long-lived stars at the end of the first step in the former alternative, equals its counterpart at the end of evolution in the latter alternative.

References

- [1] Adams, F.C., Fatuzzo, M., 1996. ApJ 464, 256.
- [2] Allende-Prieto, C., Lambert, D.L., Asplund M., 2001. ApJ 556, L63.
- [3] Barbuy, B., Nissen, P.E., Peterson, R., Spite, F. (eds.), Proceedings of Oxygen abundances in stars and implications to nucleosynthesis and cosmology (IAU Joint Discussion 8), 2001. New Astron. Rev. 45, pp. 509-588.
- [4] Binney, J., Gerhard, O., Silk, J., 2001. MNRAS 321, 471.
- [5] Bromm, V., Loeb, A., 2003. Nat 425, 812.
- [6] Bromm, V., 2004. PASP 116, 103.
- [7] Bromm, V., Larson, R.B., 2004. ARA&A 42, 79.
- [8] Caimmi, R., 1981. ApSS 79, 87.
- [9] Caimmi, R., 1982. ApSS 84, 373.
- [10] Caimmi, R., 2000. AN 321, 323. (C00)
- [11] Caimmi, R., 2001a. AN 322, 65. (C00, erratum)
- [12] Caimmi, R., 2001b. AN 322, 241. (C01)
- [13] Carney, B.W., Latham, D.W., Laird, J.B., 1990. AJ 99, 572.
- [14] Carretta, E., Gratton, R., 1997. A&AS 121, 95. (CG)
- [15] Carretta, E., Cohen, J.G., Gratton, R., Behr, B.B., 2001. AJ 122, 1469.

- [16] Chiba, M., Beers, T.C., 2000. AJ 119, 2843.
- [17] Christlieb, N., Bessell, M.S., Beers, T.C., et al., 2002. Nat 419, 904.
- [18] De Angeli, F., Piotto, G., Cassisi, S., et al., 2005. AJ 130, 116.
- [19] De Angeli, F., 2005. Private communication.
- [20] Edvardsson, B., Andersen, J., Gustaffson, B., et al., 1993. A&A 275, 101.
- [21] Feltzing, S., Holmberg, J, Hurley, J.R., 2001. A&A 377, 911.
- [22] Ferreras, I., Wyse, R.F.G., Silk, J., 2003. MNRAS 345, 1381.
- [23] Frebel, A., Christlieb, N., Norris, J.E., et al., 2006. ApJ 638, L17.
- [24] Fulbright J.P., McWilliam A., Rich R.M., 2005. Nucl. Phys. A758, 197.
Available from <astro-ph/0411041>.
- [25] Fulbright J.P., McWilliam A., Rich R.M., 2006. ApJ 636, 821.
- [26] Harris, W.E., 1996. AJ 112, 1487.
- [27] Hartwick, F.D.A., 1976. ApJ 209, 418.
- [28] Haywood, M., 2001. MNRAS 325, 1365.
- [29] Henry, R.B.C., Worthey, G., 1999. PASP 111, 919.
- [30] Huchra, J.P., Brodie, J.P., Kent, S.M., 1991. ApJ 370, 495.
- [31] Ibata, R.A., Gilmore, G.F., 1995. MNRAS 275, 605.
- [32] Ibukiyama, A., Arimoto, N., 2002. A&A 394, 927.
- [33] Israelian, G., Rebolo, R., Garcia-Lopez, R.J., et al., 2001a. ApJ 551, 833.
- [34] Israelian, G., Rebolo, R., Garcia-Lopez, R.J., et al., 2001b. ApJ 560, 535.
- [35] Iwamoto, N., Umeda, H., Tominaga, N., et al., 2002. Sci 309, 451.

- [36] Jonsell, K., Edvardsson, B., Gustafsson, B., et al., 2005. *A&A* 440, 321.
- [37] Karatas, Y., Bilir, S., Schuster, W.J., 2005. *MNRAS* 360, 1345.
- [38] Karlsson, T., 2005. *A&A* 439, 93.
- [39] Kent, S.M., 1992. *ApJ* 387, 181.
- [40] Larson, R.B., 1974. *MNRAS* 166, 585.
- [41] Larson, R.B., 1998. *MNRAS* 301, 569.
- [42] Larson, R.B., 2005. *MNRAS* 359, 211.
- [43] Li, Y., Burstein, D., 2003. *ApJ* 598, L103.
- [44] Liu, W.M., Chaboyer, B., 2000. *ApJ* 544, 818.
- [45] Mackey, A.D., van den Bergh, S., 2005. *MNRAS* 360, 631.
- [46] Malinie, G., Hartmann, D.H., Clayton, D.D., Mathews, G.J., 1993. *ApJ* 413, 633.
- [47] Marigo, P., Girardi, L., Chiosi, C., Wood, P.R., 2001. *A&A* 371, 152.
- [48] Melendez, J., Shchukina, N.G., Vasiljeva, I.E., Ramirez, I., 2005. *ApJ*, in press. Available from <astro-ph/0601256>.
- [49] Meusinger, H., Stecklum, B., Reimann, H.-G., 1991. *A&A* 245, 57.
- [50] Miller, G.E., Scalo, J.M., 1979. *ApJS* 41, 513.
- [51] Nordström, B., Mayor, M., Andersen, J., et al., 2004. *A&A* 418, 989.
- [52] Oey, M.S., 2003. *MNRAS* 339, 849.
- [53] Pagel, B.E.J., 1989. The G-dwarf Problem and Radio-active Cosmochronology. In: Beckman J.E., Pagel B.E.J. (eds.) *Evolutionary Phenomena in Galaxies*, Cambridge Univ. Press, p.201.
- [54] Pagel, B.E.J., Patchett, B.E., 1975. *MNRAS* 172, 13.
- [55] Perrett, K.M., Bridges, T.J., Hanes, D.A., et al., 2002. *AJ* 123 2490.

- [56] Prantzos, N., Silk, J., 1998. *ApJ* 507, 229.
- [57] Prantzos, N., 2003. *A&A* 404, 211.
- [58] Prochaska, J.X., Naumov, S.O., Carney, B.W., et al., 2000. *AJ* 120, 2513.
- [59] Pritzl, B.J., Venn, K.A., Irwin, M., 2005. *AJ* 130, 2140.
- [60] Rocha-Pinto, H.J., Maciel, W.J., 1997. *A&A* 325, 523.
- [61] Rocha-Pinto, H.J., Maciel, W.J., Scalo, J.M., Flynn, C., 2000. *A&A* 358, 850.
- [62] Ryan, S.G., Norris, J.E., 1991. *AJ* 101, 1865.
- [63] Sadler, E.M., Rich, R.M., Terndrup, D.M., 1996. *AJ* 112, 171.
- [64] Salpeter, E.E., 1955. *ApJ* 121, 161.
- [65] Scalo, J.M., 1986. *FCPh* 11, 1.
- [66] Schmidt, M., 1963. *ApJ* 137, 758.
- [67] Searle, L., 1972. *Star Formation and the Chemical History of Galaxies*. In: Cayrel de Strobel, G., Delplace, A.M. (eds.) *L'Age des Etoiles*, Observatoire de Paris-Meudon, p. 52.
- [68] Searle, L., Sargent, W.L.W., 1972. *ApJ* 173, 25.
- [69] Thacker, R.J., Scannapieco, E., Davis, M., 2002. *ApJ* 581, 836.
- [70] Wang, B., Silk, J., 1993. *ApJ* 406, 580.
- [71] Worthey, G., Dorman, B., Jones, L.A., 1996. *AJ* 112, 948.
- [72] Wyse, R.F.G., Gilmore, G., 1992. *AJ* 104, 144.
- [73] Zinn, R., West, M.J., 1984. *ApJS* 55, 45. (ZW)
- [74] Zoccali, M., Renzini, A., Ortolani, S., et al., 2003. *A&A* 399, 931.

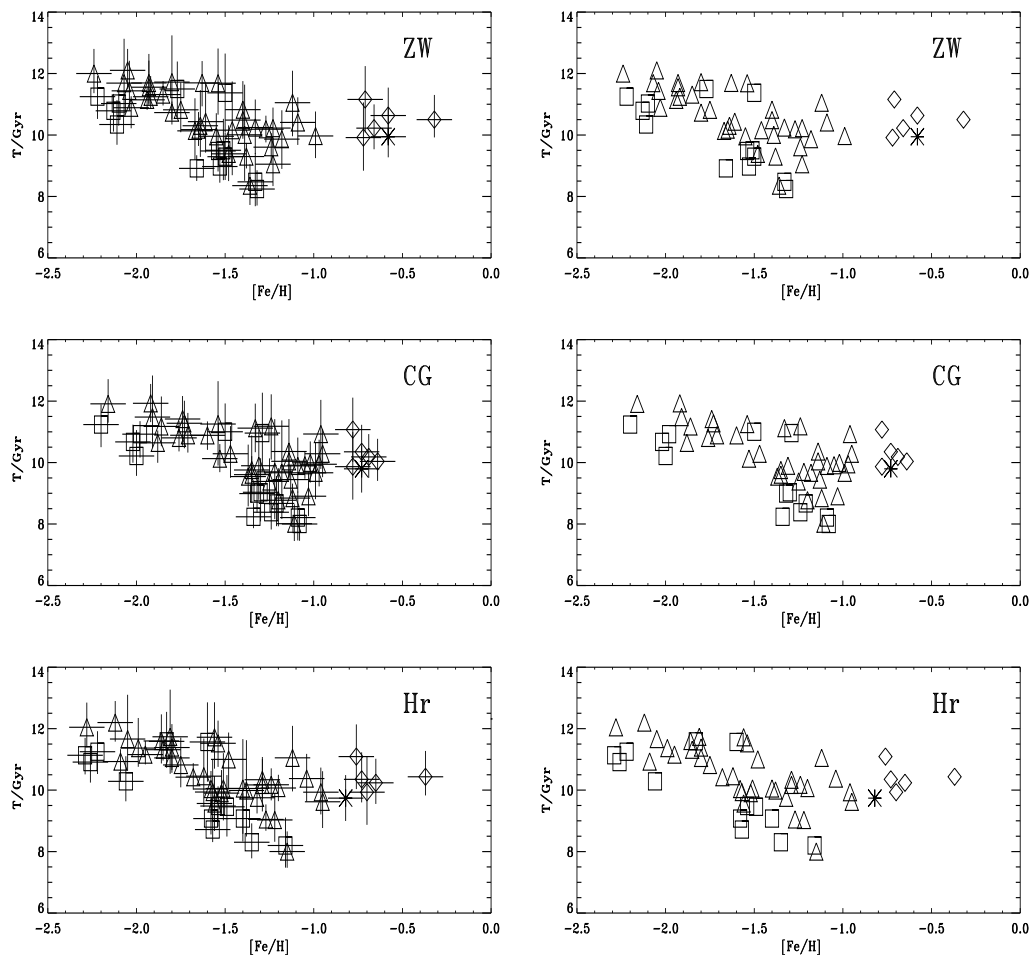


Figure 1: Empirical age-metallicity relation (EAMR) from a sample of 55 globular clusters (De Angeli et al. 2005) in terms of absolute ages (De Angeli 2005), with regard to ZW (top panels) and CG (middle panels) metallicity scales, and values from Harris catalogue (Mackey & van den Bergh 2005; bottom panels), with (left panels) and without (right panels) error bars. Morphological types: OH (old halo) - triangles; YH (young halo) - squares; BD (bulge/disk) - diamonds; NCG6366 - asterisk.

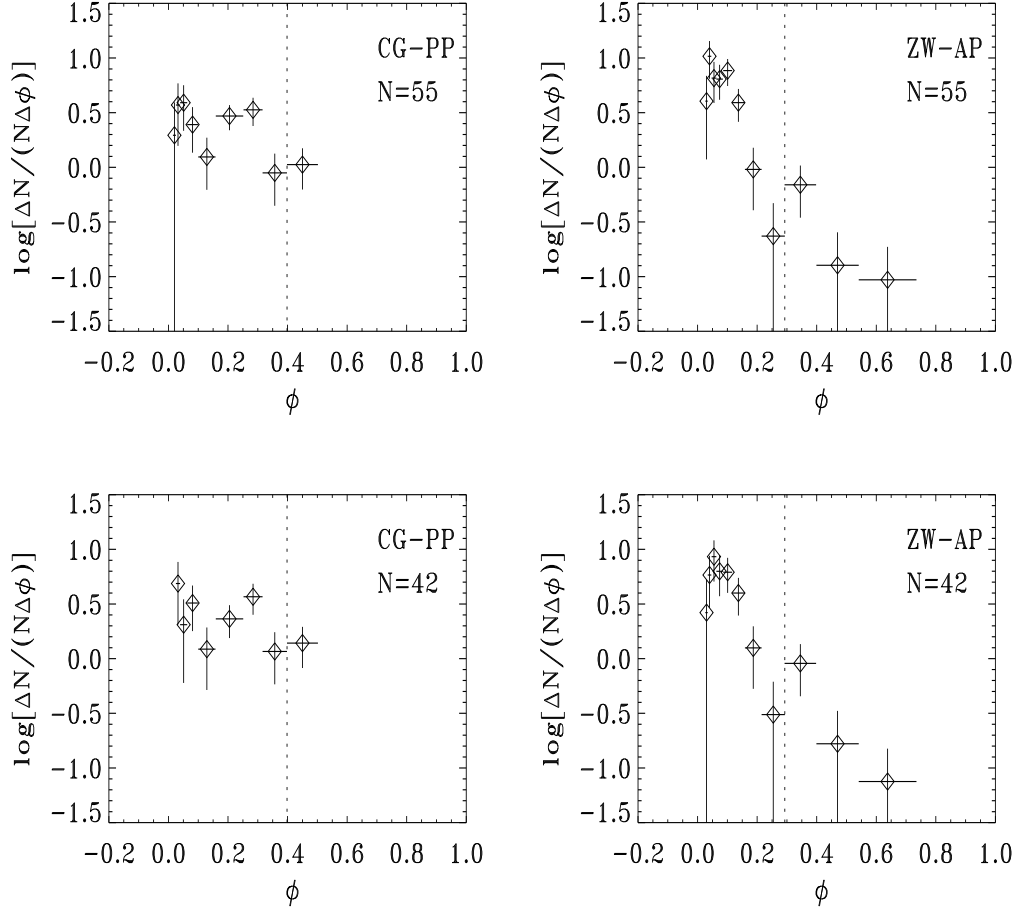


Figure 2: The empirical, differential metallicity distribution (EGD) in globular clusters, plotted with regard to a complete sample (De Angeli et al. 2005; $N = 55$, top panels) and a reduced sample ($N = 42$, bottom panels) with YH clusters removed, both in presence (left panels, CG metallicity calibration) and in absence (right panels, ZW metallicity calibration), of $[\text{O}/\text{Fe}]$ plateau, respectively. The dotted vertical line marks the transition from halo (OH, YH) to bulge/disk (BD) morphological type, $[\text{Fe}/\text{H}] = -0.8$. The distribution appears to be bimodal, with the occurrence of two maxima, close to the beginning of evolution and to the transition from halo to bulge/disk morphological type, respectively.

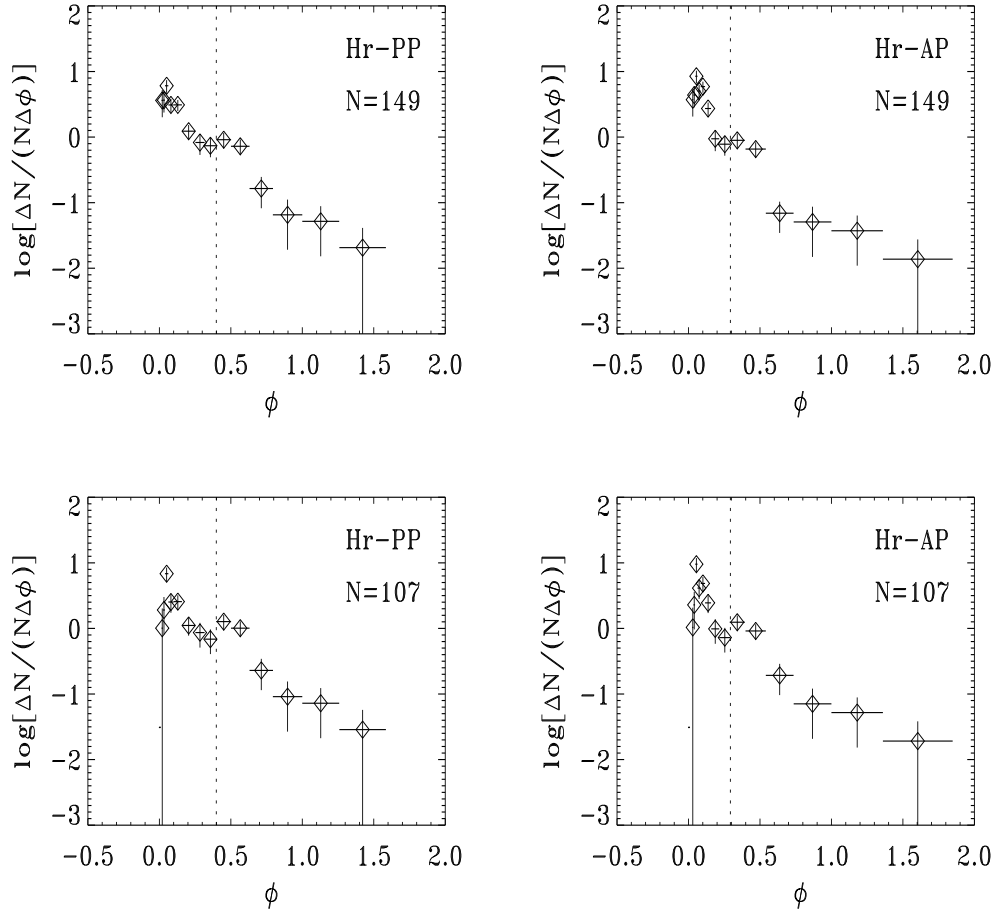


Figure 3: The empirical, differential metallicity distribution (EGD) in globular clusters, plotted with regard to a complete sample (Mackey & van den Bergh 2005; $N = 149$, top panels) and a reduced sample ($N = 107$, bottom panels) with only OH clusters retained, both in presence (left panels) and in absence (right panels) of $[O/Fe]$ plateau, respectively. The dotted vertical line marks the transition from halo (OH, YH) to bulge/disk (BD) morphological type, $[Fe/H] = -0.8$. The distribution appears to be bimodal, with the occurrence of two maxima, close to the beginning of evolution and to the transition from halo to bulge/disk morphological type, respectively.

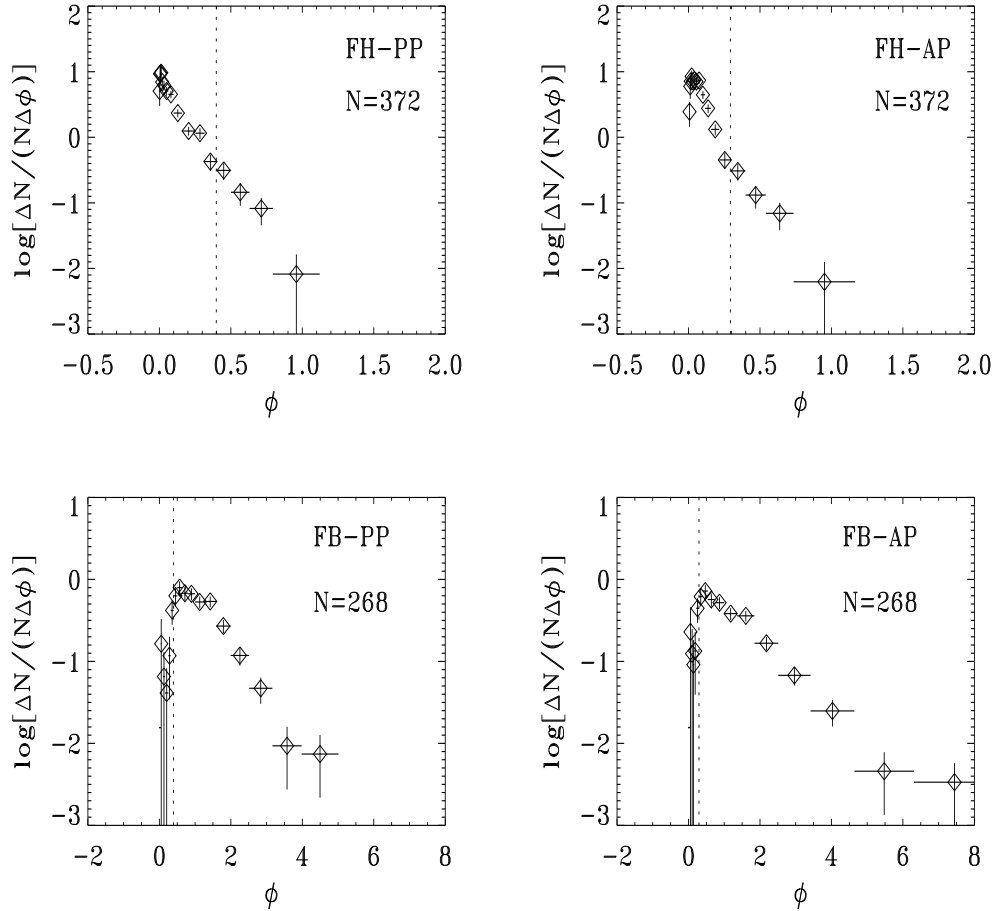


Figure 4: The empirical, differential metallicity distribution (EGD) in solar neighbourhood field halo subdwarfs (top panels), plotted with regard to a sample of 372 objects (Ryan & Norris 1991), and in K-giant field bulge stars in Baade’s Window (bottom panels), plotted with regard to a sample of 268 objects (Sadler et al. 1996), both in presence (left panels) and in absence (right panels) of $[O/Fe]$ plateau, respectively. The dotted vertical line marks the transition from halo (OH, YH) to bulge/disk (BD) morphological type, $[Fe/H]=-0.8$.

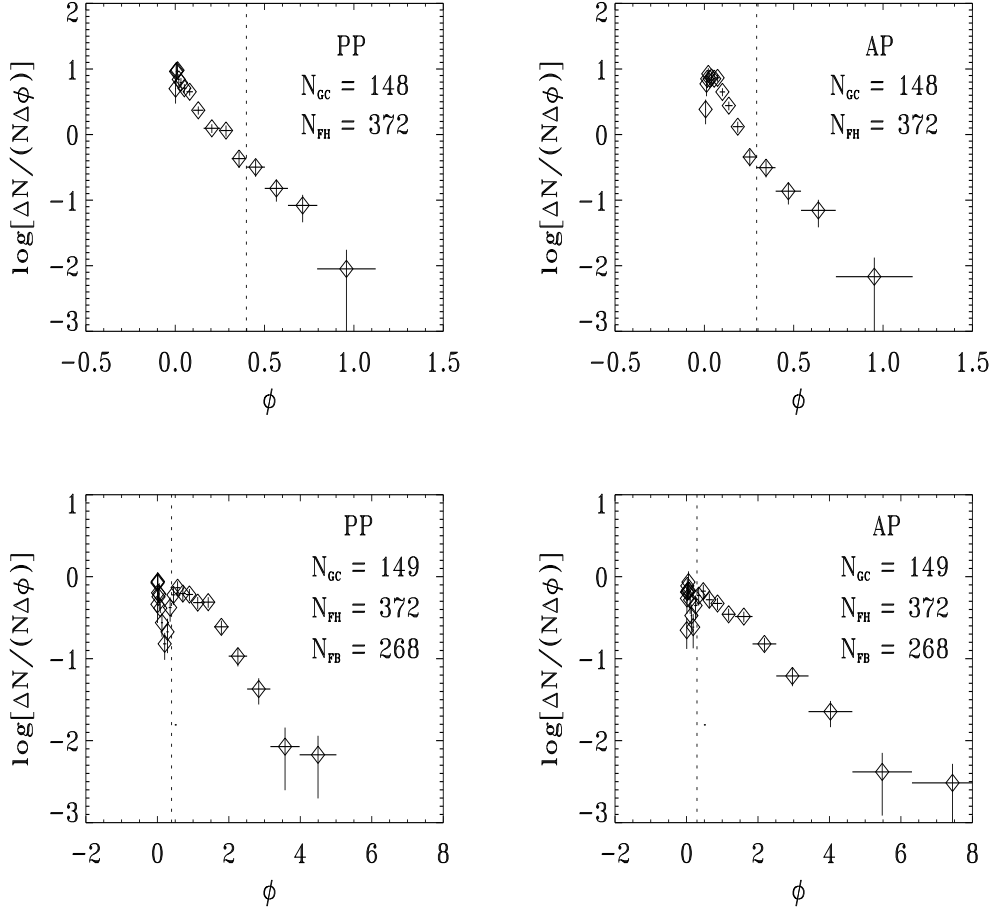


Figure 5: The empirical, differential metallicity distribution (EGD) in the light Galactic spheroid (globular clusters and field halo stars; top panels), and in the massive Galactic spheroid (globular clusters, field halo stars, and field bulge stars; bottom panels), both in presence (left panels) and in absence (right panels) of $[O/Fe]$ plateau, respectively. The distribution has been deduced using Eqs. (11), (12), and (13), from a sample of 148 (top panels) or 149 (bottom panels) globular clusters (Mackey & van den Bergh 2005), a sample of 372 field halo subdwarfs (Ryan & Norris 1991), and a sample of 268 K-giant field bulge stars (Sadler et al. 1996). The dotted vertical line marks the transition from halo (OH, YH) to bulge/disk (BD) morphological type, $[Fe/H]=-0.8$.

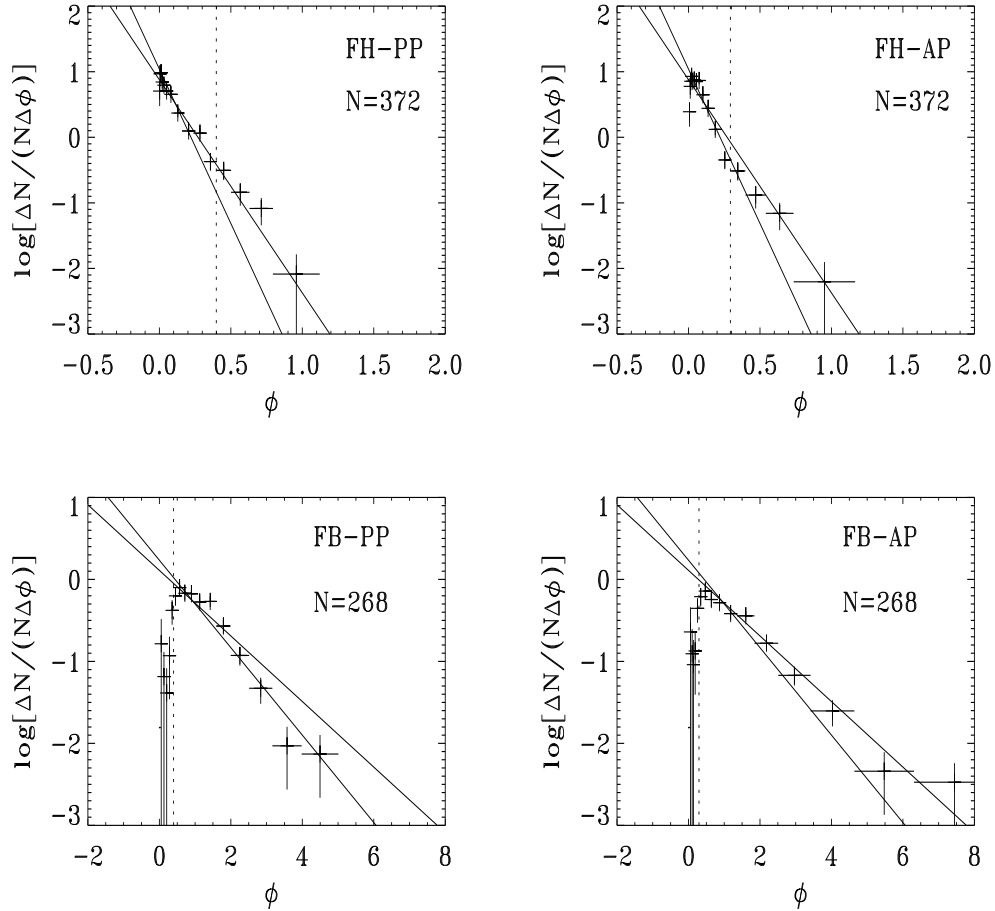


Figure 6: Comparison between theoretical (TGD) and empirical differential oxygen abundance distribution (EGD) in halo (top panels) and bulge (bottom panels) field stars, both in presence (left panels) and in absence (right panels) of [O/Fe] plateau, respectively. The straight lines correspond to homogeneous models, H1-H2 (top panels) and B1-B2 (bottom panels) defined in Tabs. 7 and 8. Crosses represent the data and related uncertainties, as in Fig. 4. The dotted vertical line marks the transition from halo (OH, YH) to bulge/disk (BD) morphological type in globular clusters, $[\text{Fe}/\text{H}] = -0.8$.

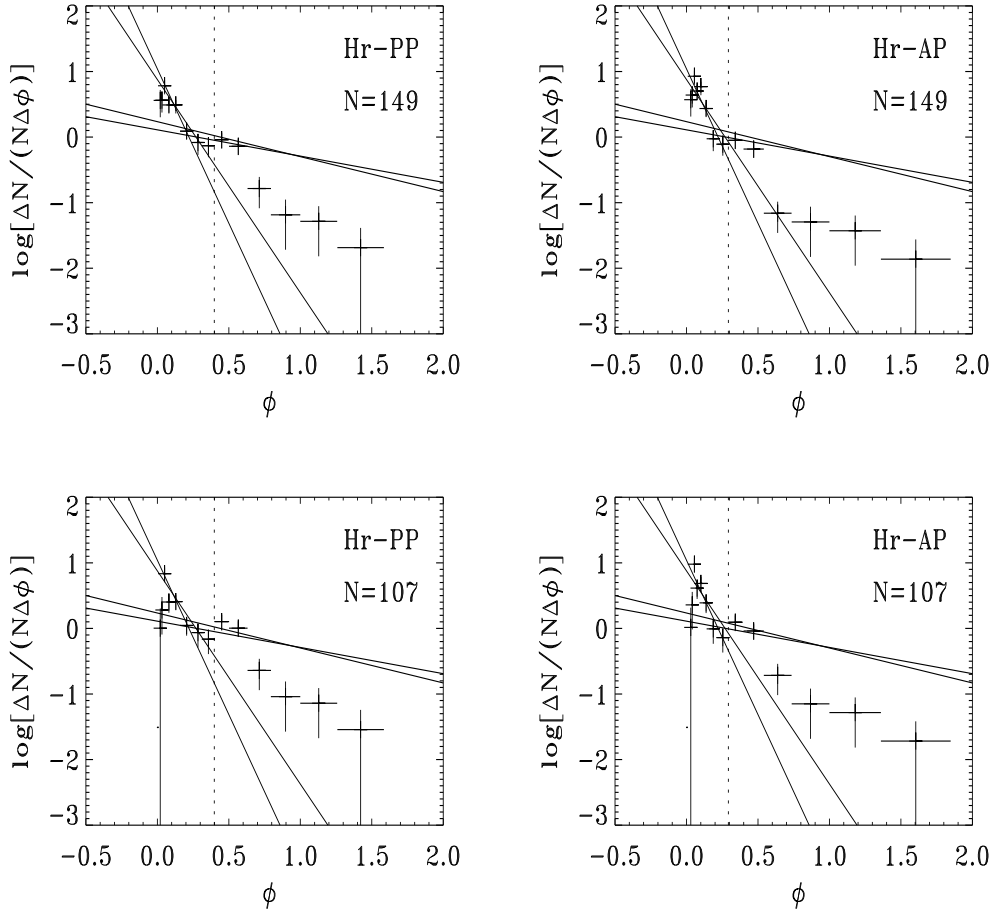


Figure 7: Comparison between theoretical (TGD) and empirical differential oxygen abundance distribution (EGD) in globular clusters of all morphological types (top panels) and with only old halo and bulge/disk objects retained (bottom panels), both in presence (left panels) and in absence (right panels) of $[\text{O}/\text{Fe}]$ plateau, respectively. The straight lines correspond to homogeneous models, H1-H2 (more inclined) and B1-B2 (less inclined), respectively, defined in Tabs. 7 and 8. Crosses represent the data and related uncertainties, as in Fig. 3. The dotted vertical line marks the transition from halo (OH, YH) to bulge/disk (BD) morphological type in globular clusters, $[\text{Fe}/\text{H}]=-0.8$.

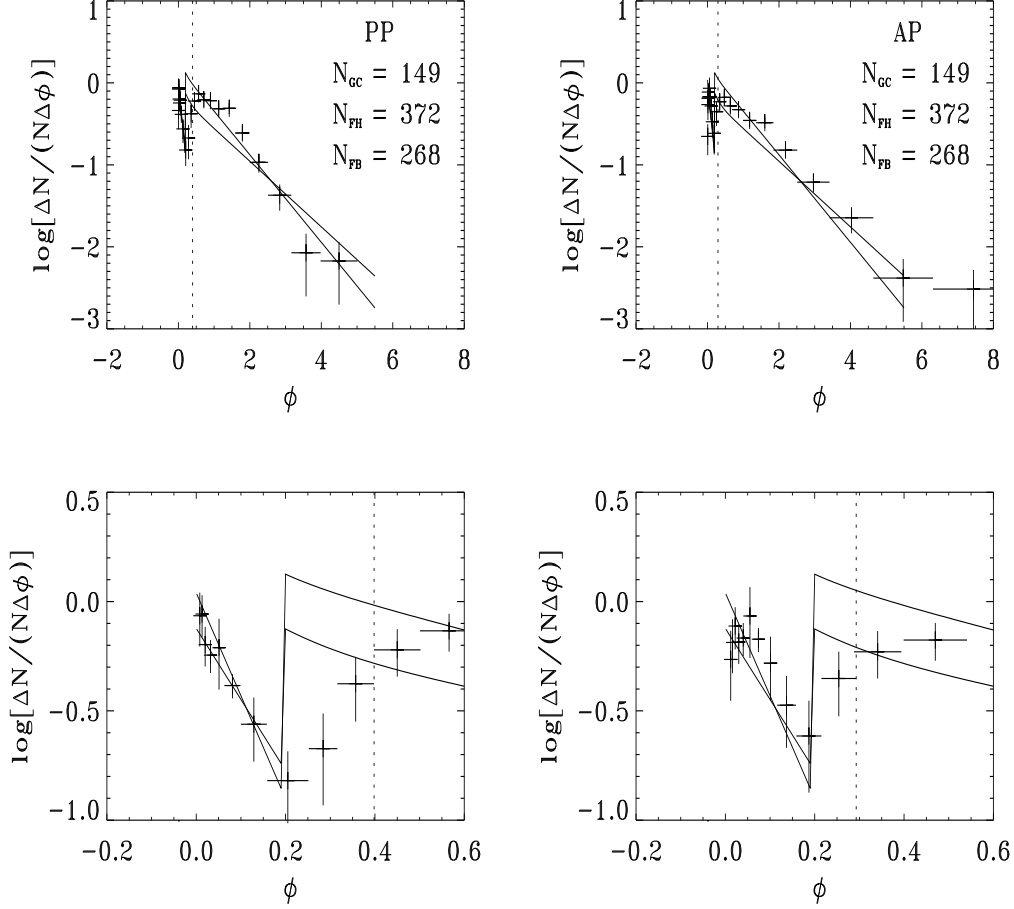


Figure 8: Comparison between theoretical (TGD) and empirical differential oxygen abundance distribution (EGD) in the Galactic spheroid (top panels) and zoomed for low oxygen abundance (bottom panels), both in presence (left panels) and in absence (right panels) of $[O/Fe]$ plateau, respectively. The curves correspond to models, H1, B1; H2, B2; defined in Tabs. 7 and 8 and combined via Eq. (27). Crosses represent the combination of the data and related uncertainties via Eqs. (13), as in Fig. 5 (bottom panels). The dotted vertical line marks the transition from halo (OH, YH) to bulge/disk (BD) morphological type in globular clusters, $[Fe/H] = -0.8$.

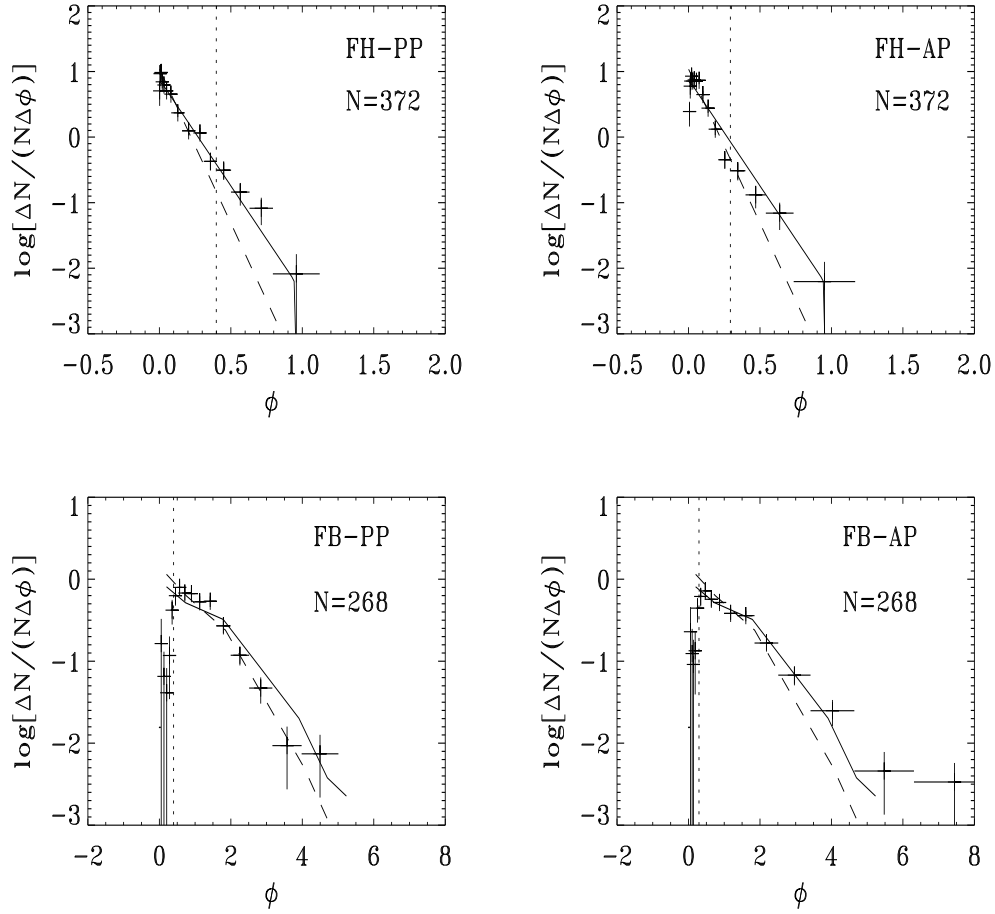


Figure 9: Comparison between theoretical (TGD) and empirical differential oxygen abundance distribution (EGD) in halo (top panels) and bulge (bottom panels) field stars, both in presence (left panels) and in absence (right panels) of $[O/Fe]$ plateau, respectively. Full curves correspond to inhomogeneous models H1 (top panels) and B1 (bottom panels), and dashed curves to H2 (top panels) and B2 (bottom panels), defined in Tab. 9. Crosses represent the data and related uncertainties, as in Fig. 4. The dotted vertical line marks the transition from halo (OH, YH) to bulge/disk (BD) morphological type in globular clusters, $[Fe/H] = -0.8$.

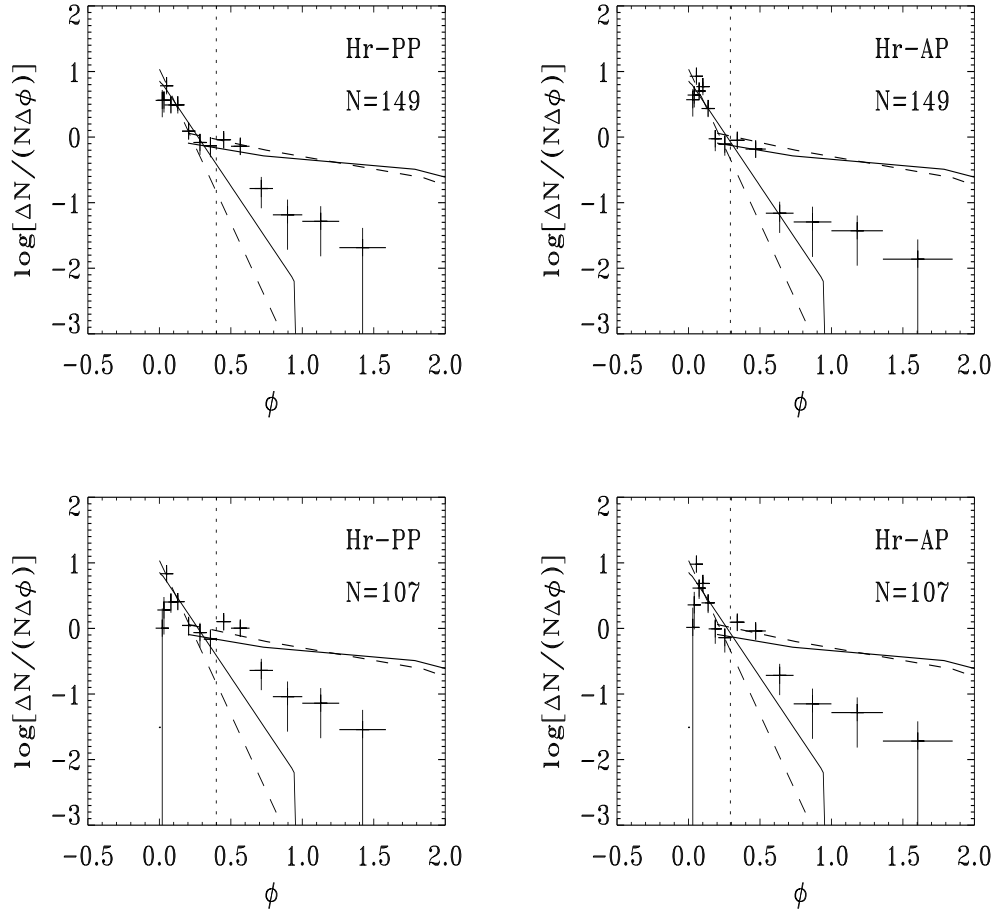


Figure 10: Comparison between theoretical (TGD) and empirical differential oxygen abundance distribution (EGD) in all sample globular clusters (top panels) and only old halo and bulge/disk objects (bottom panels), both in presence (left panels) and in absence (right panels) of $[O/Fe]$ plateau, respectively. Full curves correspond to models H1 and B1, and dashed curves to H2 and B2, where H curves have larger slope with respect to B curves. Crosses represent the data and related uncertainties, as in Fig. 3. The dotted vertical line marks the transition from halo (OH, YH) to bulge/disk (BD) morphological type in globular clusters, $[Fe/H] = -0.8$.

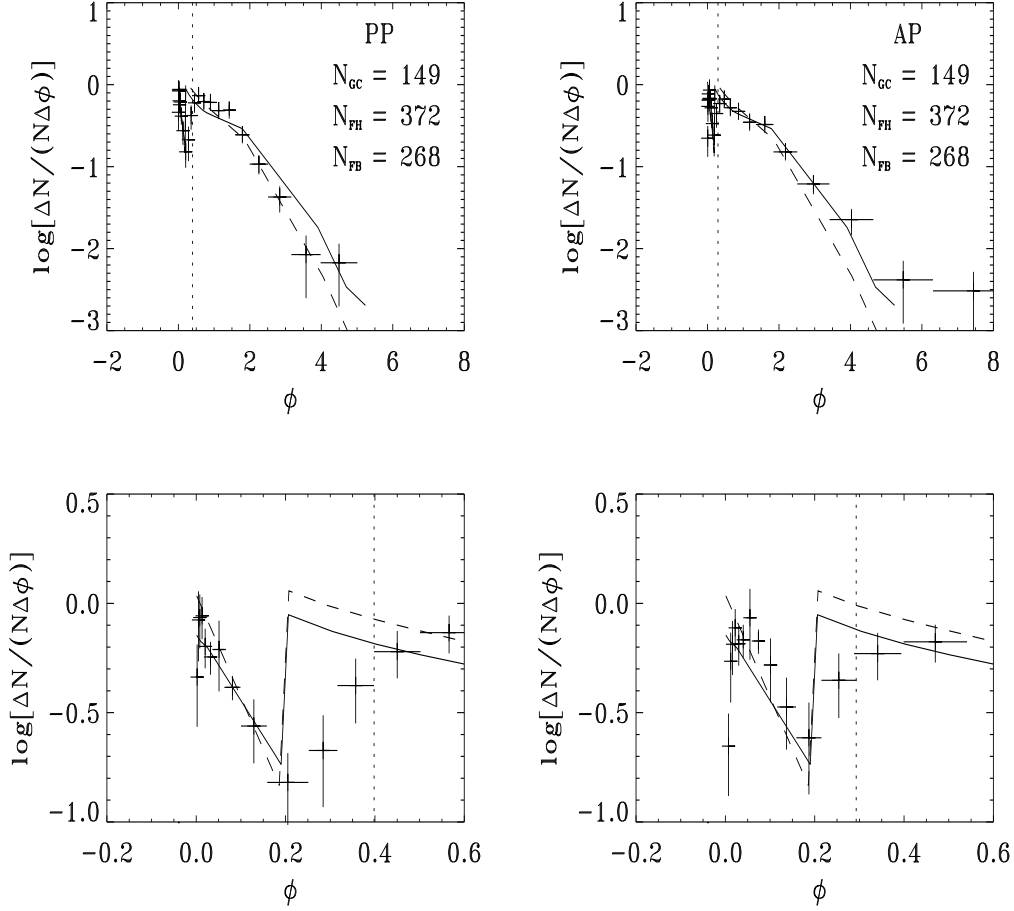


Figure 11: Comparison between theoretical (TGD) and empirical differential oxygen abundance distribution (EGD) in the Galactic spheroid (top panels) and zoomed for low normalized oxygen abundances (bottom panels), both in presence (left panels) and in absence (right panels) of $[O/Fe]$ plateau, respectively. Full and dashed curves correspond to models H1, B1; H2, B2; respectively, listed in Tabs. 7-9 and combined via Eq. (26). Crosses represent the combination of the data and related uncertainties via Eqs. (13), as in Fig. 5 (bottom panels). The dotted vertical line marks the transition from halo (OH, YH) to bulge/disk (BD) morphological type in globular clusters, $[Fe/H] = -0.8$.

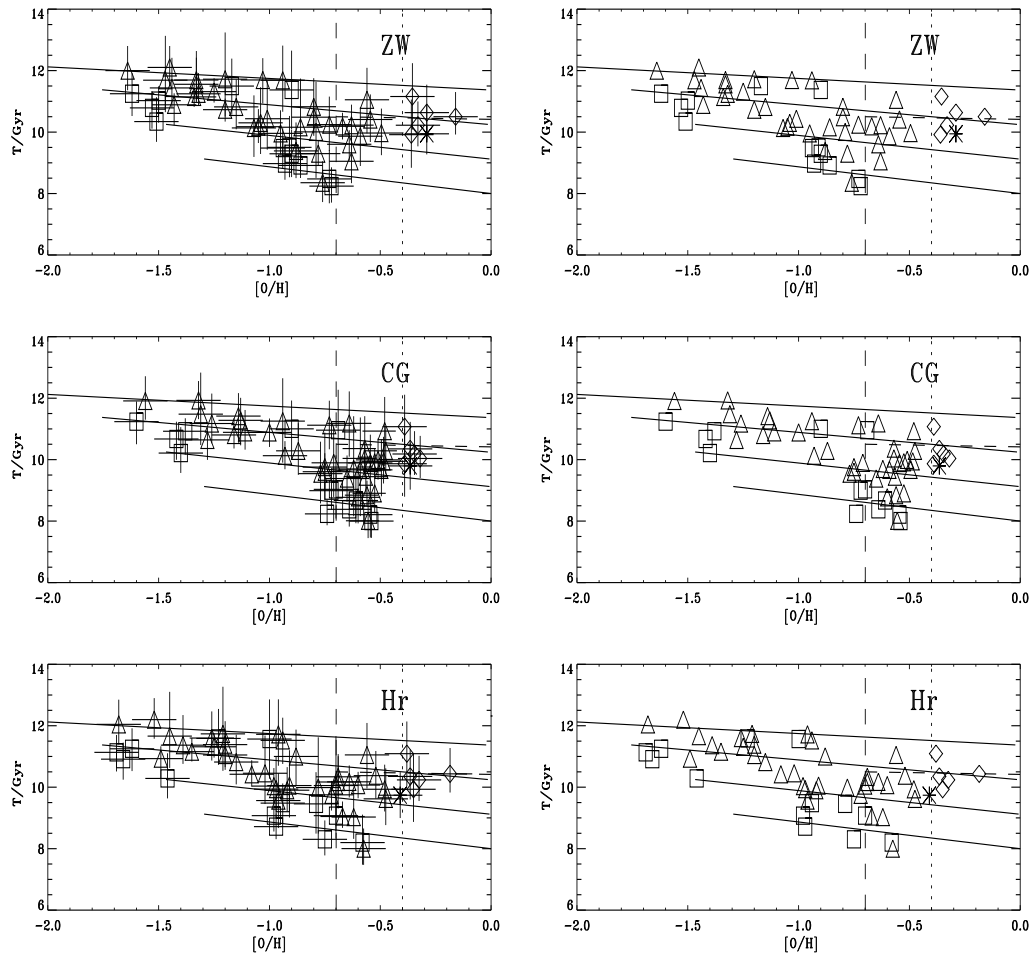


Figure 12: Comparison between empirical (EAMR) and theoretical age-metallicity relation (TAMR) in presence of $[O/Fe]$ plateau, according to Eq. (1). The data come from a sample of 55 globular clusters (De Angeli et al. 2005) but expressed in terms of absolute ages (De Angeli 2005). Other captions as in Fig. 1. Full and dashed curves are related to models H1 and B1, respectively. Halo star formation begins at $([O/H], T/\text{Gyr}) = (-3, 12.5)$ and ends at $(0, 8.0)$, within four time steps, $\Delta T/\text{Gyr} = 1.125$. Bulge star formations begins at $(-0.70, 10.5)$ and ends at $(0.74, 10.0)$, within four time steps, $\Delta T/\text{Gyr} = 0.125$. The last three steps are out of scale on the right, and cannot be shown. The dotted vertical line marks the transition from halo (OH, YH) to bulge/disk (BD) morphological type in globular clusters, $[Fe/H] = -0.8$. The dashed vertical line marks the minimum in the differential oxygen abundance distribution (EGD) in the Galactic spheroid (Fig. 8), $\phi = 0.20$ or $\log \phi = [O/H] = -0.70$.

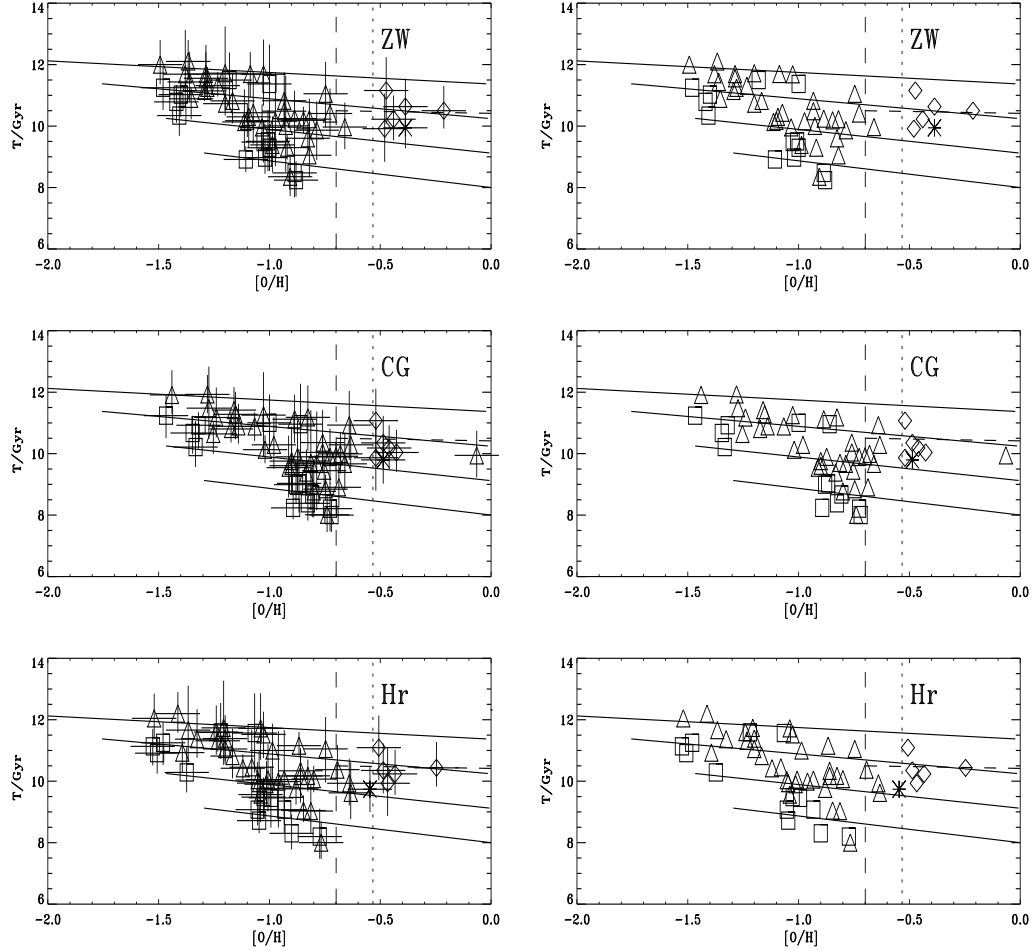


Figure 13: Comparison between empirical (EAMR) and theoretical age-metallicity relation (TAMR) in absence of $[\text{O}/\text{Fe}]$ plateau, according to Eq. (2). The data come from a sample of 55 globular clusters (De Angeli et al. 2005) but expressed in terms of absolute ages (De Angeli 2005). Other captions as in Fig. 1. Full and dashed curves are related to models H1 and B1, respectively. Halo star formation begins at $([\text{O}/\text{H}], T/\text{Gyr}) = (-3, 12.5)$ and ends at $(0, 8.0)$, within four time steps, $\Delta T/\text{Gyr} = 1.125$. Bulge star formations begins at $(-0.70, 10.5)$ and ends at $(0.74, 10.0)$, within four time steps, $\Delta T/\text{Gyr} = 0.125$. The last three steps are out of scale on the right, and cannot be shown. The dotted vertical line marks the transition from halo (OH, YH) to bulge/disk (BD) morphological type in globular clusters, $[\text{Fe}/\text{H}] = -0.8$. The dashed vertical line marks the minimum in the differential oxygen abundance distribution (EGD) in the Galactic spheroid (Fig. 8), $\phi = 0.20$ or $\log \phi = [\text{O}/\text{H}] = -0.70$.